Calcium doped ZnO ETL Effect on the Performance of Inverted P3HT: PCBM based Polymer Solar Cell

Rahel Eshetu Abebe

A Thesis Submitted to

The Department of Materials Science and Engineering

School of Mechanical, Chemical, and Material Engineering

Presented in Partial Fulfillment for the Requirement of Degree of Masters in Materials Science and Engineering

Office of Graduate Studies

Adama Science and Technology University

June, 2023

Adama, Ethiopia

Calcium doped ZnO ETL Effect on the Performance of Inverted P3HT: PCBM based Polymer Solar Cell

Rahel Eshetu Abebe

Advisor: Fekadu Gochole Aga (PhD)

Co-Advisor: Solomon Tiruneh Dibaba (PhD)

A Thesis Submitted to
The Department of Material Science and Engineering
School of Mechanical, Chemical, and Material Engineering

Presented in Partial Fulfillment for the Requirement of Degree of Masters in Materials Science and Engineering

Office of Graduate Studies
Adama Science and Technology University

June, 2023

Adama, Ethiopia

DECLARATION

I declare that this thesis work entitled **"Calcium doped ZnO ETL Effect on the Performance of Inverted P3HT:PCBM based Polymer Solar Cell"** is my own work and has not been submitted to any university for a similar purpose. The references used in this thesis are duly recognized by proper citations.

_____	_____	_____
Name of Student	Signature	Date

RECOMMENDATION OF ADVISOR

I, the major advisor/supervisor of this thesis, hereby certify that I have closely advised/supervised the student while developing this thesis and read the draft thesis work entitled **"Calcium doped ZnO ETL Effect on the Performance of Inverted P3HT:PCBM based Polymer Solar Cell"** prepared under my guidance by Rahel Eshetu Abebe. Therefore, I recommend the submission of the thesis to the department for further review and evaluation.

_____	_____	_____
Major Advisor/Supervisor	Signature	Date
_____	_____	_____
CO - Advisor/Supervisor	Signature	Date

APPROVAL SHEET

We, the undersigned, members of the Board of Reviewers of the thesis open defense by Rahel Eshetu Abebe have read and evaluated the thesis work **"Calcium doped ZnO ETL Effect on the Performance of Inverted P3HT:PCBM based Polymer Solar Cell"** and assessed the understanding of the candidate about the proposed research. This is, therefore, to certify that the thesis is accepted and we recommend the implementation of the thesis.

Chairperson	Signature	Date
Reviewer 1	Signature	Date
Reviewer 2	Signature	Date

Finally, approval and acceptance of the thesis are contingent upon the submission of its final copy to the Office of Postgraduate Studies (OPGS) through the Department Graduate Council (DGC) and School Graduate Committee (SGC).

Department Head	Signature	Date
School Dean	Signature	Date

ACKNOWLEDGEMENT

First, I would like to thank God, for letting me through all the difficulties. I have experienced your guidance day by day. I also acknowledge Adama Science and Technology University (ASTU) for giving me the chance of MSc opportunity and research fund to accomplish this research. I would like to express my sincere gratitude to my advisor Dr. Fekadu Gochole who made this work possible by bringing his considerable experience and knowledge to this project. His guidance and advise carried me through all the stages of doing my work and writing my thesis, I am extremely grateful for your assistance and suggestion throughout my project. I am very grateful for Dr. Gebisa Bekele, Dr. Dinsefa Mensur, Mr. Demeke Tesfaye and Ms. Kidan for their encouragement and support. I am sincerely express my gratitude to Dr. Newaymedihn Tegegn Abera for letting me work on material physics and polymer lab at Addis Ababa University. Finally, I would like to give my warmest thanks to my family and friends for their continuous support and understanding when undertaking my project, your prayer helps me survive all the stress from this year and not letting me give up.

TABLE OF CONTENTS

LIST OF TABLES

LIST OF FIGURES

LIST OF ACRONYMS

Acronyms	Definition
BHJ PSCs	Bulk heterojunction polymer solar cells
Ca:ZnO	Calcium doped zinc oxide
CBM	Conduction band minimum
D/A	Donor/accepter
E_F	Fermi energy
EIS	Electrochemical impedance spectroscopy
ETL	Electron transport layer
FF	Fill factor
HOMO	Highest occupied molecular orbital
HTL	Hole transport layer
iPSCs	Inverted polymer solar cells
ITO	Indium tin oxide
J_{sc}	Short circuit current density
J-V	Current density versus voltage
LED	Light emitting diode
MTF	Multi-tier framework
MoO_3	Molybdenum tri-oxide
OSCs	Organic solar cells

PCBM	[6,6]-phenyl–C_{61}– butyric acid methyl ester
PCE	Power conversion efficiency
P3HT	Poly (3 – hexyl thiophene)
PEDOT: PSS	Poly (3,4-ethylenedioxythiophene): poly-styrene sulphonate
P_{in}	Input power
P_{out}	Power output
P_{max}	Maximum power
PL	Photoluminescence
R_S	Series resistance
R_{sh}	Shunt resistance
SEM	Scanning electron microscopy
UV-Vis-NIR	Ultra violet visible near-infrared
V_{oc}	Open circuit voltage
WF	Work function
XRD	X-ray diffraction

ABSTRACT

In this research study, P3HT:PCBM bulk heterojunction (BHJ) inverted polymer solar cells (PSCs) were successfully fabricated. Calcium-doped Zinc oxide was prepared using a low-temperature sol-gel process. Their morphological, electrical, and optical characteristics in response to varying concentrations of calcium in host ZnO were investigated. The results showed that the inverted polymer solar cell devices utilizing Ca:ZnO films as electron transport layer exhibited a better performance as compared with pure ZnO films. The inverted polymer solar cells incorporating a 3% Ca:ZnO ETL displayed a notably improved efficiency of 3.25% compared to a pristine ZnO ETL efficiency of 1.31%. The photovoltaic performance of the iPSCs with Ca:ZnO ETLs can be attributed to several factors, including adjustable band gaps, high optical transparency, enhanced electron mobility, increased electrical conductivity, and optimized surface morphology. The findings also demonstrated result shows that the Ca:ZnO interfacial layers improved electron extraction and successfully suppressed photogenerated carrier recombination within solar cell devices. This groundbreaking development represents a significant step forward in the field of bulk heterojunction polymer solar cells with inverted structures, paving the way for further advancements in this area of sustainable energy research.

Keywords*: polymer solar cell, calcium-doped ZnO, power conversion efficiency, surface morphology, electron extraction, carrier recombination, and mobility*

CHAPTER ONE

1. INTRODUCTION

1.1. Background of the study

Recently, the global energy consumption has increased every year due to the rapid growth of the population. The world's energy mostly comes from fossil fuels like coal, oil, and gas. Consuming fossil fuels cause environmental damage by producing greenhouse gases and land degradation during exploration and extraction. The result in the occurrence and spread of tropical diseases which hurt humans, animals, and plants. These horrific conditions can potentially harm delicate ecosystems (Landrigan et al., 2018; Organization, 2016). Furthermore, the energy generated from these sources becomes expensive. To meet the expanding energy demand and reduce environmental harm a new, clean, and limitless energy sources are also needed. The best way to deal with this effect is to introduce sustainable energy sources, including geothermal, hydropower, solar, wind, and biogas (Khalate et al., 2018; Slama et al., 2016).

One of the most promising way to supply future generations growing energy needs with eco-friendly energy is the conversion of sunlight into electricity, which offers a sustainable electricity supply (Khordehgah et al., 2019; Sampaio et al., 2020; Zahid et al., 2022). The development of photovoltaic (PV) technology is still exciting, with advances being made quickly in the choice of materials, device engineering, and production methods. The development of green and sustainable energy sources has sparked a growing interest in this topic. Organic photovoltaic (OPV) cells are less expensive and have the potential to replace established photovoltaic technology. It is the driving force behind efforts to find new potential for PV cell innovation (Sampaio & González, 2017).

Bulk heterojunction (BHJ) polymer solar cells (PSCs) have attracted the interest of numerous research groups over the past 20 years form OPV technology. A conjugated semiconducting polymer as donor and fullerene derivatives or non-fullerene materials as acceptor blends are used as photon absorbers in BHJ PSCs to generate exciton. Most importantly, the LUMO of the donor polymer should be at least 0.3 eV higher than the LUMO of the corresponding acceptor material to provide enough driving force to break the electron-hole (e-h) pair binding energy and lead to charge separation (Chen et al., 2015; Zhao et al., 2016). Photon absorption and exciton generation, exciton diffusion, charge

separation, and charge collection are the four steps for the working principle of the BHJ PSC (Devižis et al., 2021; Jarosz et al., 2022).

The most commonly used device structures for a BHJ PSC are conventional and inverted. The typical multilayered structure of a conventional PSCs is composed of an electrode, a hole transport layer, an active layer, an electron transport layer, and a low work function electrode (Fanady, 2021). Unfortunately, typical conventional PSCs have low stability due to oxygen and moisture in ambient air. It has suggested that PSCs stability and performance problems can resolved by inverting their structural design because it reduces the exposure of the active layer to atmospheric oxygen and moisture, which can cause degradation of the organic materials and increase the charge extraction. The inverted PSCs (iPSCs) have an electrode, an ETL, a photoactive layer, a HTL, and a high-work-function electrode device structure. Due to their noticeably environmental stability compared to conventional solar cells, solution-processed inverted BHJ PSCs have attracted much more interest in the past ten years (Sampaio & González, 2017).

Even though, the device structure and active layer material both significantly affect power conversion efficiency (PCE), the ETLs utilized as an interfacial layer between the photoactive layer and the cathode also play a crucial role (Wei et al., 2017). The creation of ohmic contact, alteration of internal electric field, and decrease in carrier recombination rate (Wang et al., 2015), enable effective exciton dissociation, and charge extraction or inducing interfacial charge redistribution processes.

Because of its relatively high electron mobility, wider band gap, good transparency over the visible spectral range, and environmental durability, ZnO has attracted much interest in being used as the electron transport layer (Huang et al., 2018; Tang et al., 2017). Excellent pyroelectric and piezoelectric capabilities are displayed. Additionally, by preventing the UV light-induced photodegradation of organic components in inverted devices, the ZnO layer can improve the operational stability of PSCs. Another benefit of using ZnO as the buffer layer is to treat using the solution approach and thermal annealing at a low temperature (Shah et al., 2023). There is a light absorption of ZnO in the visible light region results in fast recombination of photogenerated charges, which can limit their efficiency in optoelectronic devices. Other drawbacks are their high sensitivity to processing conditions, such as deposition temperature, pressure, and atmosphere. The defects in ZnO may affect their electrical and optical properties. It can also affect the

adhesion and durability of the ZnO layer, leading to delamination or cracking (Lee et al., 2016).

The structural, optical, and electrical properties of ZnO varied due to doping with a group II elements, such as Mg, Be, and Sr (Istrate et al., 2019; Polat et al., 2017). The band gap of Mg tuned the ZnO effectively adjust the materials electrical and optical properties for specific applications. Similarly, when Sr is doped to ZnO, the band gap can be reduced, with potentially improve the efficiency of PSCs. The particle size and optical properties of ZnO nanostructures can also improve by using Calcium and beryllium (Mahdhi et al., 2018).

Calcium-doped ZnO is a modified form of the ZnO compound, where some Zn^{2+} ions(0.88Å) were replaced with Ca^{2+} ions(1.14Å). Some potential uses of calcium-doped ZnO include photocatalytic applications, its high photocatalytic activity makes it suitable for water treatment, and photodegradation of pollutants. Another significant application of calcium-doped ZnO is in gas sensing devices, the addition of calcium ions enhances sensitivity and selectivity towards specific gases enabling the development of more efficient and accurate gas sensors for various industries (Ghiloufi et al., 2016). It is a promising candidate for electronic devices, such as field-effect transistors (FETs), solar cells, and light-emitting diodes (LEDs) (Jaballah et al., 2020). The enhanced electrical and optical properties of calcium-doped ZnO make it suitable for producing transparent conductive films. These films can used in various optoelectronic applications, such as touch screens and flat-panel displays (Sekicek & Oral, 2021).

Generally, calcium-doped ZnO has improved properties that make it suitable for various applications. Consequently, this versatile material has immense potential for contributing to developing innovative and futuristic technologies. In this work, a comparative study has performed to measure the overall iPSCs efficiency of Ca-doped ZnO and pristine ZnO film deposited using spin-coating and fabricated using the sol-gel method.

1.2. Statement of Problem

Sol-gel-prepared zinc oxide (ZnO) shows good optical transparency in visible light and is a highly appropriate material for the electron transport layer. At the same time they effectively blocking holes migration from active layer. It is post-treated with low-temperature annealing (150–200°C) to enhance the development of crystalline ZnO and minimize high-surface defects that may impair device performance after being deposited

as thin films (Sreedharan & Das, 2022). Despite these efforts, ZnO films prepared by low temperatures sol-gel still have a high degree of surface roughness and mismatch between the conduction band of ZnO and the LUMO of acceptor material in the active layer. This can reduces the amount of contact they have with the photoactive layer. It is also susceptible to lower charge mobility and electrical conductivity, which leads to reduced photovoltaic performance and limits its application for efficient and stable iPSCs (Borse et al., 2018).

To successfully overcome the limits of sol-gel-prepared ZnO films and achieve high-performance iPSC devices, structural modification of ZnO is carried out. To date, the doping of organic material into ZnO or the deposition of organic or inorganic materials as a second interfacial layer on top of ZnO film used to study interface engineering or interfacial modification in ZnO. Both techniques can reduce surface traps and defects in ZnO, improve interfacial contact with the photoactive layer, change the work function (WF) of the electrode, increase the conductivity of ZnO, and suppress recombination losses, which is advantageous for increasing photovoltaic performance (Amakali et al., 2020; Ismail et al., 2019). In addition, to alleviate these problems doping of alkaline earth metal elements causes the alteration of the grain size of ZnO thin films at the nanoscale, reduces surface defects in sol-gel ZnO, and improves interfacial contact with the active layer (Sekicek & Oral, 2021). This work opens the path to investigates calcium (Ca) as a dopant in host ZnO with a simple sol gel preparation method for ETL to improve the performance of iPSC devices.

1.3. Objectives

1.3.1. General Objective

The overall objective of this study is to synthesize calcium-doped ZnO (Ca:ZnO) electron transport layer by using sol-gel method to determine its effect on inverted P3HT: PCBM based BHJ PSCs.

1.3.2. Specific Objective

- To synthesize pristine ZnO and calcium-doped ZnO solution by varying concentrations of Ca (1, 2, 3, 4, and 5) wt%.
- To characterize the synthesized Ca:ZnO for structural, morphological, optical, electrical, and electrochemical properties using XRD, FTIR, SEM, UV-Vis spectroscopy, PL, conductivity, and EIS, respectively.

- To fabricate the inverted BHJ PSCs with a device structure of Glass/ITO/ZnO/ P3HT:$PC_{61}BM$/MoO_3/Al and ITO/Ca:ZnO/P3HT:$PC_{61}BM$/MoO_3/Al, and analyzing the photo-conversion (J-V) performance of the fabricated iPSCs devices.
- To determine the charge mobility enhancement of the iPSCs device after the incorporation of Ca.

1.4. Significance of the Study

Despite a rapidly increasing demand for electricity in Ethiopia, only a small portion of households access it. According to the Multi-Tier Framework (MTF) of the World Bank, just 44% of all residences have access to any power, and 56% of families use non-renewable energy sources for their daily energy usage (Padam et al., 2018). Even for individuals wired to the grid, power outages frequently occur and last for prolonged periods. The primary reasons for the frequent power outages include a lack of supply, scheduled outages, and transmission and distribution lines that have insufficient capacity. Those that use non-renewable energy also lead to the emission of CO_2, which is a significant contributor to anthropogenic greenhouse gases worldwide, resulting in rising global temperatures (Gnangoin et al., 2022).

Solar energy is a viable option for guaranteeing all sections of the country through clean and renewable energy sources, especially rural ones, access electricity because it covers a large area. As a result, it ensures safe and dependable solar energy and it also provides cost-effective power supplies for people remote from the primary electricity grid.

1.5. Scope of the Study

In this work, Ca doping ZnO ($Zn_{1-x}Ca_xO$, x=0.01, 0.02, 0.03, 0.04 and 0.05) were synthesized through a simple and environmentally friendly sol-gel method and deposited using spin coater. The Ca:ZnO films were characterized by using different characterization, such as XRD, FTIR, SEM, UV-Vis, PL, EIS and conductivity. The effect of Ca:ZnO on the photovoltaic performance and charge mobility of iPSCs also evaluated. The study is limited in modifying the ZnO ETL in P3HT: PCBM based iPSCs to achieve the goals via the doping process of Ca ions in ZnO.

CHAPTER TWO

2. LITERATURE REVIEW

2.1 Organic Solar Cell

Renewable energy like hydroelectricity, biomass, wind power, and solar energy have the most tremendous potential for the need of energy requirement. Among these renewable energy, solar cells has capabilities to produce high amount of energy. As shown in the Fig. 2.1 below, are three main types of solar cells; silicon-based solar cells, thin film solar cells, and emerging technologies-based solar cells. Among these organic solar cells are one of the emerging technologies of solar cells which have much interest as a potential substitute for their inorganic counterparts (Le Donne et al., 2019; Muhammad et al., 2019). OSCs offer some distinct advantages compared to other cell types, such as cost-effectiveness, simple processing procedures, being light weight, semi-transparency options, and environmentally friendly. They also have an advantage over conventional inorganic solar cells due to their fast and inexpensive roll-to-roll (R2R) manufacture, lightweight, and construction on flexible substrates (Qu & Forrest, 2018; Wei et al., 2018). Organic semiconducting materials have a substantially higher absorption coefficient. Furthermore, a power conversion efficiency (PCE) of more than 18% for OSCs is achieved, which is comparable to commercial silicon solar cell efficiency, via years of rigorous research conducted (Liu et al., 2020; M. Zhang et al., 2021).

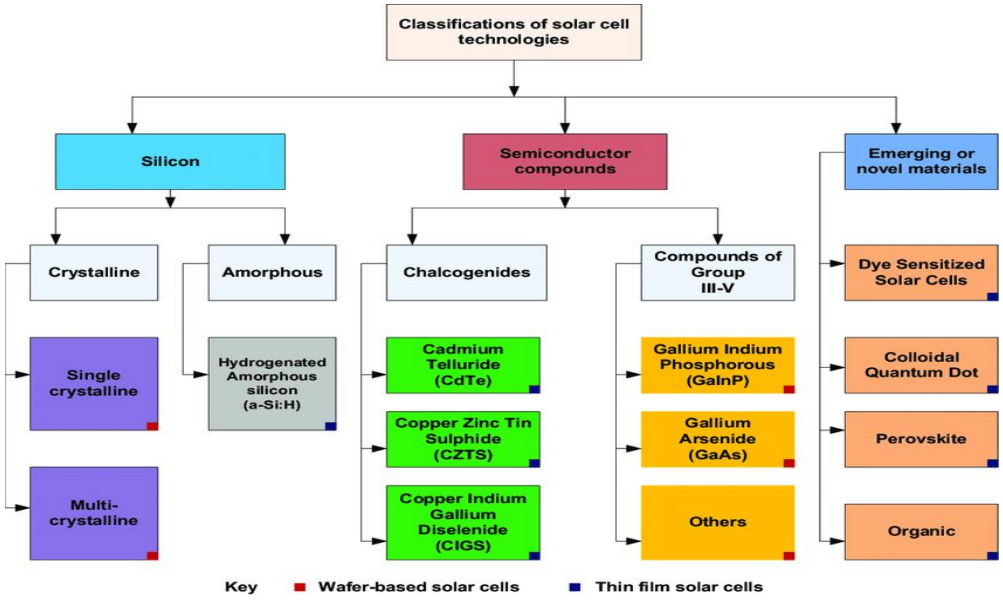

Figure 2.1 Solar cell classification on the primary active material (Ibn-Mohammed et al., 2017).

Small molecules and polymers are the two main groups into which organic solar cells can divide. Polymer solar cells use conjugated polymers as the active layer in the device. Small molecule solar cells, on the other hand, use small molecules as the active layer in the device. The optical band gaps are almost equivalent with inorganic semiconductor valence band-LUMO and conduction band-HOMO. The energy band gap in inorganic semiconductors is comparable to the HOMO-LUMO gap in organic semiconductors. Organic semiconductors typically have band gaps between 1 and 3 eV (Rasmussen & Pomerantz, 2007).

In order to increase the devices power conversion efficiencies (PCE), a bulk heterojunction (BHJ) design is developed. In BHJ organic solar cells, the acceptor is dispersed more uniformly throughout the donor matrix to create an interpenetrating network of acceptors and donors. This results in a three-dimensional network of donor-acceptor interfaces that facilitate more efficient exciton dissociation, increasing photoinduced charge generation. A conjugated polymer solution and tiny molecules, typically fullerene, comprise a typical active layer. For organic solar cells, the most popular and well-optimized active layer is a combination of P3HT (Poly (3 – hexyl thiophene)) and PCBM ([6,6]-phenyl–C_{61}– butyric acid methyl ester). P3HT:PCBM organic solar cells have a high device efficiency, and because of their consistency and

manufacturing simplicity, they have grown to be an essential paradigm for researching different device parameters in organic solar cells (Feng et al., 2023; Li et al., 2019).

2.2 Operating Principle

The four fundamental steps for the operating process of the BHJ PSCs device divided into; i) photon absorption and exciton generation; ii) exciton diffusion and splitting; iii) charge transfer; and iv) charge collection (Devižis et al., 2021). The donor material in BHJ PSC devices typically absorbs light, such as a conjugated polymer. Energy of photon will accelerate an electron from the HOMO to the LUMO. In an organic semiconductor, the electron-hole pair is attracted to one another by Coulomb attraction because of the low dielectric constant and localized electron and hole wave functions with a binding energy of 0.1–1.4 eV, the resulting electron-hole pair is known as a Frenkel exciton (Choy, 2012).

The donor-acceptor interface is where the exciton must separate into the free charge carriers (the electrons and holes) due to a sufficient potential energy drop (Cheng et al., 2018; Classen et al., 2020). Each carrier must be carried to the appropriate electrode through the bicontinuous interpenetrating channel after splitting into free charge carriers and avoiding recombination and charge trapping. These processes may hampered by thermalization loss (Abramavicius et al., 2016; Andersson & Kemerink, 2020), insufficient amount of energy for exciton splitting, charge recombination, and other constraints and losses (Menke et al., 2018).

There are two types of excitons, namely Frenkel exciton and Wannier–Mott exciton. Frenkel exciton has a typical binding energy of 0.1 to 1 eV. They found in organic solar cells or materials with a relatively small dielectric constant. While Wannier–Mott excitons binding energy is usually much less than that of a hydrogen atom, typically on the order of 0.01eV. Wannier–Mott excitons are found in semiconductor crystals with small energy gaps and high dielectric constants (Classen et al., 2020; Romanin et al., 2022).

i. Photon Absorption and exciton generation

Conjugated polymers can absorb light at the maximum of their absorption spectrum with a very thin photoactive layer, in contrast to their inorganic silicon, which needs thicknesses of hundreds of micrometers. The thickness of the polymer-based photoactive layer is limited to 100 nm due to the poor charge-carrier mobility found in the majority of

polymers, which causes only 60% of the incident light to be absorbed in the absorption maximum (excluding the electrode's back reflection) (Oseni & Mola, 2019; Wu et al., 2019). It is noteworthy that narrowing the band gap of donor polymers can boost PCE by increasing the amount of light absorbed (Cheng & Yang, 2020; Liu et al., 2018).

ii. Exciton diffusion and charge dissociation

At the donor/acceptor interface of organic semiconductors, photogenerated holes, and electrons are strongly bound by the Coulomb force. It is broken by the energy difference in LUMO between the materials acting as the donor and acceptor, leading to the excitons' dissociation (Dimitrov & Durrant, 2014). To achieve effective charge separation, a high degree of mixing between donor and acceptor materials is preferred because the exciton diffusion length in organic semiconductors is short (usually 10 nm) (Sampaio et al., 2020; Zhang et al., 2019). Clarke & Durant reported the exciton diffusion length ranges from 5 to 20 nm for different conjugated polymers and fullerene acceptors (Cowan et al., 2010). while the exciton diffusion length range from 20nm to 50nm for non-fullerene acceptors (Firdaus et al., 2020). Therefore, the photoactive layers thickness is very crucial for effective charge creation and exciton separation at the donor-acceptor interface (Stolterfoht et al., 2016). However, once they are free of their mutual Coulomb attraction, they either recombine or separate into free-charge carriers (Bässler & Köhler, 2015; Vithanage et al., 2013). Efficient exciton dissociation at the interface is necessary for efficient charge transmission. At the interface, electrostatic forces are generated by the difference in HOMO and LUMO between the donor and acceptor layers. When the right materials are chosen, these variations provide an electric field that effectively breaks up exciton into electrons and holes (Ito et al., 2013). Additionally, the materials with greater LUMO levels accept the free electrons, while the materials with lower HOMO levels accept the free holes. Unfortunately, when they move toward the electrodes, these free charge carriers have the potential to recombine or become trapped in an unorganized interpenetrating organic material.

iii. Free charge carrier transport

The charges should be carried in the direction of the appropriate electrodes after the exciton dissociates into free charge carriers. In organic semiconductors, the majority of charge carrier transit occurs through hopping from one localized state to the next. Due to the Fermi level difference between the electrodes, free charge carriers are transported

toward their respective electrodes by an internal electric field (Bhat et al., 2010). The internal electric field that is produced by a high work function(WF) anode and a low WF cathode often defines the cell's *Voc* (Elumalai et al., 2013). Either carrier diffusion or drift driven by an electric field is responsible for the movement of free-charge carriers. The recombination of free charge carriers, before they reach the anode and cathode, is the main barrier to the efficient passage of these carriers to the electrodes. The transportation of the charge carriers, as well as the losses brought on by charge carrier recombination, are governed by the charge carriers' mobility in the photoactive layer (Choy, 2012). The Coulomb potential nevertheless holds electrons and holes in place in the case of low-mobility materials. Due to this, they are unable to resist their attraction to one another and recombine before charge collection at the electrodes. As a result, the solar cell suffers a serious loss in photogenerated current.

The path length of photogenerated electrons and holes is in direct proportion to the thickness of the photoactive layer. Charge carrier recombination increases as the photoactive layer gets thicker, resulting in a substantial loss in the device's performance (Cowan et al., 2010). Thus, competition between carrier sweep-out by the internal field and the loss of photogenerated carriers by recombination are significant issues to overcome for high-efficiency devices.

iv. Collection of the charge carriers at the electrodes

Photogenerated charge carriers that do not recombine are finally extracted from the photoactive layer to the respective electrodes. The potential barrier at the photoactive layer electrode interface must be reduced to maximize the extraction of charges. In an inverted polymer solar cell, the work function of the anode should be matched to the highest occupied molecular orbital (HOMO) of the donor material (Chang et al., 2013). If the WFs match well as described, then the contacts are said to be Ohmic contacts. Contrary to this, if there is a mismatch between the anode and cathode with that of donor HOMO or acceptor LUMO, respectively, then no Ohmic contacts would be established, resulting in low performance of the solar cells (Liu et al., 2016).

The charge collection at the respective electrodes concludes the steps from absorption of light to generation of photocurrent. The PV performance characteristics such as Jsc, *Voc*, and FF are reliant on photocurrent generation.

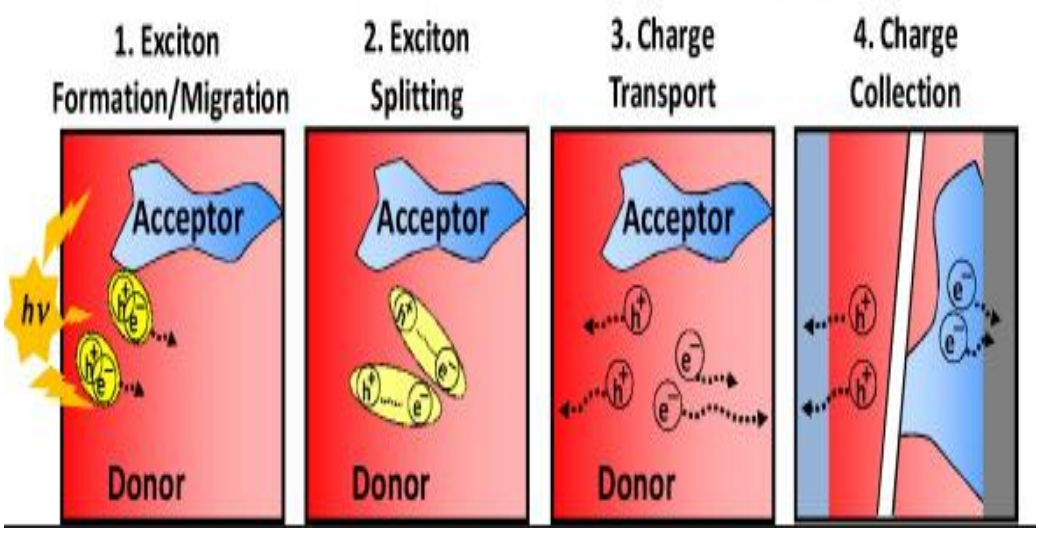

Figure 2.2 shows (a) Exciton generation (b) Exciton diffusion and exciton dissociation and (d) Charge collection (Opitz et al., 2009).

2.3 Device structure of BHJ PSCs

Conventional BHJ PSCs contain transparent conducting oxide (TCO) anodes, hole transport layers, photoactive layers, electron transport layers, and a top cathode. In particular, the use of an efficient HTL with high optical transparency, good chemical stability, and good electron-blocking ability between the anode and photoactive layer facilitates better hole transport, consequently improving device performance (Jørgensen et al., 2012; Pan et al., 2013). In typical PSCs, poly(3,4-ethylenedioxy-thiophene): poly(styrene sulfonate) (PEDOT: PSS) is a widely used HTL material because it easily deposit by spin-coating and shows the high work function (WF) ~ 5.2 eV, which is well matched to the highest occupied molecular orbital (HOMO) level of many of the polymers used as active layers (X. Zhou et al., 2022). This structure has been used in the realization of devices with very good performance, reaching a PCE of around 9%. Despite these good efficiency reports, which, are far from being reproducible, such a structure suffers from several drawbacks: a low work function metal electrode is used on top of a device like Al. However, it undergoes very fast oxidation when exposed to air and moisture, losing their conductivity, and suddenly turning a working device into a faulty one. Moreover, the PEDOT: PSS is acidic in nature and it corrodes the ITO electrode, and thus detrimental to the underlying metal oxide layer, which undergoes fast degradation (Elumalai et al., 2013). Therefore, to improve device stability inverted polymer solar cell is developed.

The inverted structure has several advantages over the standard structure. It was first exploited in the fabrication of organic light-emitting diodes, also initially referred to as an "upside-down" structure. The improved device stability is one benefit of iPSCs, as the organic charge selective layers in the inverted structure can offer better protection against environmental moisture and oxygen and improved charge collection efficiency is another benefit, as the inverted shape can lower carrier recombination at the metal electrode contact, increasing device efficiency. In inverted structure the top anode is made of certain high-work-function metals (such as Au, Ag, and Al) integrated with a stable metal oxide HTL with the bottom transparent ITO electrode modified with low WF materials acting as the cathode or ETL. Due to the vertical phase separation between the donor and acceptor, inverted PSCs may exhibit better power conversion efficiency through device optimisation than conventional solar cells.

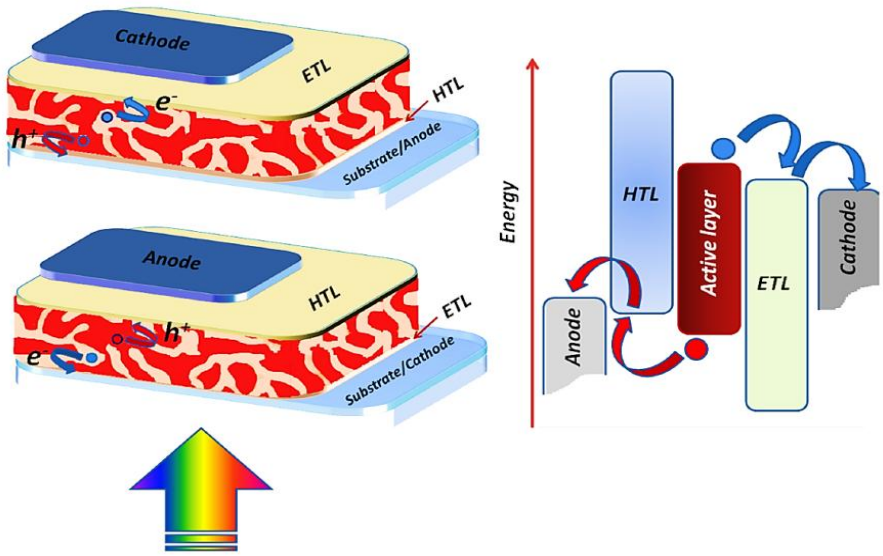

Figure 2.3 Schematic of standard (top) and inverted (bottom) geometries for a BHJ photovoltaic cell, Along with an energy level diagram of the constituent layers (Lattante, 2014).

A typical active layer is made up of a mixture of small molecules, mainly fullerene, and conjugated polymers. The most popular and well-optimized active layer for organic solar cells is P3HT:PCBM mixure. These polymer solar cells have a high device efficiency, and because they are reliable and simple to make, they are a useful model for researching different device parameters in organic solar cells. Ameri et al. Works using a P3HT:PCBM photoactive layer conventional solar cell and an inverted analog; P3HT:

PCBM blend undergoes a vertical phase separation during the process of film formation, resulting in a stratified structure in which a PCBM-rich layer is formed on the bottom of the film and a P3HT-rich layer is formed on the top. As the electrons mainly travel inside the PCBM phase and the holes mainly travel inside the P3HT phase towards the respective electrodes, they found that the inverted device performed about 15% better than the conventional one. The inverted structure is characterized by a self-assembled ETL (hole blocking) as the electron extraction electrode (bottom) and an HTL (electron-blocking) as the hole extraction electrode (top), thus both increasing the charge extraction efficiency and reducing the bimolecular recombination at the electrodes (Chambon et al., 2012; Wantz et al., 2014).

The introduction of A-D-A structured non-fullerene acceptors (NFAs) have emerged as a promising alternative due to their superior properties. One advantage of NFAs is their higher thermal stability compared to fullerene derivatives. This allows for more stable device performance under elevated temperatures, which is important for practical applications (Yuan et al., 2019). NFAs also exhibit broader optical absorption properties, particularly in the near-infrared region, which can increase the efficiency of light harvesting in PSCs. Furthermore, NFAs are easier to tune in terms of their molecular energy levels, which can be crucial for efficient charge transfer in OPVs. The introduction of NFAs with narrow bandgap and small interfacial energy offset in the HOMO level has been shown to significantly improve the performance of OPVs, leading to higher power conversion efficiency (R. Wang et al., 2019; Zhang et al., 2020). Some of NFAs are 3,9-bis(2-methylene-(3-(1,1dicyanomethylene)-indanone))−5,5,11,11-tetrakis(4hexylphenyl)-dithieno[2,3d:2’,3’d’]-s-indaceno[1,2-b:5,6-b’]dithio phene (so-called ITIC) and its derivatives (IT-M, IT-Th, IT-F, IT-4F), IT-M andY6 are some of nonfullerene materials used in PSCs. These NFAs have been extensively studied and have shown promising results in improving the efficiency of PSCs.

Table 2.1 Photovoltaic parameters for non-fullerene acceptor

Device	V_{OC} [V]	J_{SC} [mA cm^{-2}]	FF [%]	PCE [%]	Ref.
A (ZnO/PBDB-TF:Y6)	0.834	25.2	72	15.1	(Zhang et al., 2017)
B (ZnO/*c*-PCBSD/PBDB-TF:Y6)	0.838	25.2	73	15.4	(Hong et al., 2021)
C (ZnO/*c*-PCBSD/PBDB-TF:Y6:*c*-PCBSD)	0.844	25.4	0.75	16.1	(Hong et al., 2021)

Photovoltaic parameters in BHJ PSCs

The photovoltaic parameters that determine the efficiency of the solar cell can be extracted from J-V curves and are summarized as:

i. Short circuit current density (J_{sc})

The current measured when the device is connected in a short circuit is known as the J_{sc}. The J_{sc} has been demonstrated to be sensitive to the type of solvent, film shape, and deposition technique (Moulé & Meerholz, 2008). Due to the rise in charge separation interfaces, the development of BHJ has improved J_{sc} but it is still considerably lower than that of their inorganic equivalents, though. This is primarily caused by a spectral mismatch between the active layer's absorption spectrum and that of sunlight, as well as by organic materials' low carrier mobilities because J_{sc} is directly related to the efficiencies of light absorption, exciton generation and dissociation, charge transport, and charge collection at the electrodes (Tang et al., 2021).

ii. The open-circuit voltage (V_{oc})

It is the maximum voltage available from a solar cell, and this occurs at zero current. The V_{OC} corresponds to the amount of forward bias on the solar cell due to the bias of the solar cell junction with the light-generated current. In BHJ PSCs in which charge separation at the D/A interface occurs very efficiently the energy difference between the acceptor LUMO and the donor's HOMO determines the open-circuit voltage primarily. Furthermore, it depends on the D/A blend morphology as well as the morphology and nature of the electrode. Specifically, it is determined by the difference between the quasi-

Fermi levels of holes (E_F,h) and electrons (E_F,e) when illuminated, assuming that barrier-free connections are created with the electrodes (Potscavage Jr et al., 2009; Ratcliff et al., 2011).

iii. Fill Factor

The "fill factor "(FF) is the parameter that, in conjunction with Voc and Jsc, determines the maximum power from a solar cell. The FF is defined as the ratio of the maximum power from the solar cell to the product of Voc and Jsc.

$$FF = \frac{Vmax \times Imax}{Voc \times Jsc} \quad (1)$$

Where V_{max}: maximum voltage, I_{max}: maximum current, Voc: open circuit voltage, and Isc: short circuit current.

The parasitic series resistance (R_s) and shunt resistance (R_{sh}) of the solar cell both influence FF. The electrodes' bulk conductivity, the active and interfacial layers, and the contact resistance between them all play a role in determining R_S. The thin films and their interfaces quality affects R_{sh} (Potscavage Jr et al., 2009). Small R_{sh} results from the recombination and trapping of charge carriers during their transit through the cell as well as the loss of charge carriers through leakage pathways such as pinholes in the films, which can impair device performance. All three factors associated with the device can be strongly impacted by the type of electrical contact between the BHJ layer and the electrodes, and those interfaces can be modified by adding the right interfacial layers to the device.

iv. Power Conversion Efficiency

PCE represents the ratio where the output electrical power at the maximum power point on the J-V curve is divided by the incident light power. The power conversion efficiency of organic solar cells is given as in Eqn. 2.

$$PCE(\eta) = \frac{P_{out}}{P_{in}} = \frac{FF \times J_{SC} \times V_{OC}}{P_{in}} \quad (2)$$

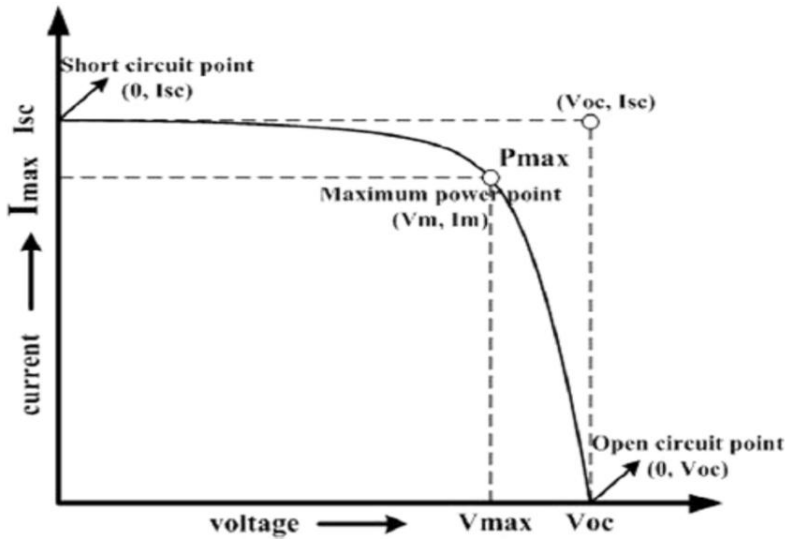

Figure 2.4 J-V curve for photovoltaic cell (El-Ahmar et al., 2016).

In fullerene-based PSCs, device stability over time has been greatly affected. A typical PSCs degradation curve can be divided into three regimes: 1) burn-in, which refers to the initial period of rapid degradation; 2) long-term, which shows relatively slower and linear degradation; and 3) failure, which shows fast and complete degradation until device failure. Several factors influence PSCs stability (Wang et al., 2018; Zhang et al., 2017). The active layer architecture is frequently thermodynamically metastable, allowing large aggregates to form easily via thermal or light induction, especially under long-term illumination. To address this issue, molecular stabilization of the donor/acceptor blend is critical. Furthermore, the interfacial material is the main influencer of device stability because it's impacted by environmental factors such as oxygen and humidity. The selection of solvent material also affect the morphology of the cell and it reduce its stability.

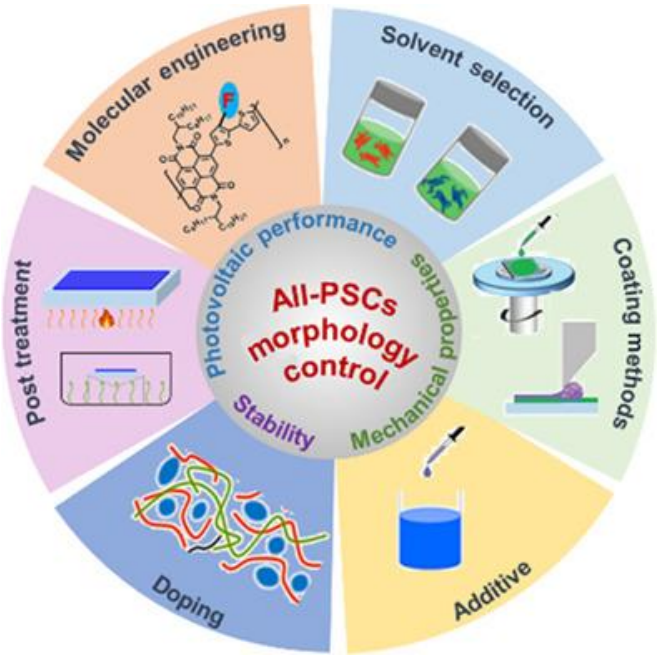

Figure 2.5 Schematics of the impact of morphology control in PSCs (K. Zhou et al., 2022)

2.4 Interfacial material

The performance and stability of PSCs are greatly influenced by the interfaces within the electrodes and the photoactive layer. In PSCs, charge transport is critical for optimal device performance. Efficient, and balanced charge transfer decreases current losses from recombination and series resistance losses under high irradiances. A suitable interfacial layer can boost the selectivity of the corresponding electrode for holes and electrons while also adjusting the energy barrier height between the active layer and the electrodes and play a significant part in balancing the rates of electron and hole collection at both corresponding electrodes. In terms of their electronic, electrical, and optical properties, effective interfacial materials should meet a number of criteria. They should (i) allow the formation of Ohmic contacts between the electrodes and the active layer; (ii) have the proper energy levels to improve charge selectivity for the corresponding electrodes; (iii) have a large bandgap to confine excitons in the active layer; (iv) have enough conductivity to lower resistive losses; and (v) have low absorption in the Vis-NIR wavelengths to reduce optical losses; (vi) the capacity to process from solution and at low temperatures, (vii) strong film-forming capabilities, and (viii) cheap cost of production (Xie & Würthner, 2017; Yip & Jen, 2012).

For use as cathode and anode interfacial materials, solution-processable metal compounds, particularly metal oxides and transition metal chelates, have potential due to their advantages of high charge carrier mobility, suitable work function, low cost, and high environmental stability. Hole-transporting materials (HTL) have been widely used and proven successful (Yang et al., 2020), while various metal oxides (i.e., TiO_2, SnO_2, ZnO) and organic electrolytes (i.e., PFN, PFN-Br, PEIE) are all potential electron transporting layer (ETL) candidates to improve optoelectronic properties of PSCs and enable effective extraction/transport of electrons generated by the active layer (Huang et al., 2020; Noh et al., 2020).

2.4.1 Hole transport layer (HTL)

The following electronic qualities should be present in the materials used in the HTL: (i) Ohmic contact at the active layer/anode interface requires an energy level that matches the HOMO of the donor material in the active layer. and (ii) a large band-gap (Eg> 3eV) with a conduction band (CB) higher than the LUMO level of either the donor or acceptor materials for successfully preventing electron leakage to the anode. A lot of materials mett the requirements. PEDOT: PSS is the most widely used HTL with several commercial varieties available (Yip & Jen, 2012). Some formulations of PEDOT: PSS are highly acidic with a pH of 1-3 and together with residual water or moisture from the air this is a possible source of corrosion, especially in conjunction with low work function metals such as aluminum or calcium used in normal type geometry devices, but may also be implicated in the degradation of the ITO electrode. (Voroshazi et al., 2011). recently investigated the role of PEDOT: PSS in cathode oxidation for polymer solar cells with normal geometry (Lizin et al., 2013) and found that it greatly accelerates oxidation due to its hygroscopic nature. In a later more comprehensive study, it was found that even in a dry inert atmosphere PEDOT: PSS accelerates degradation presumably due to residual humidity that can diffuse through the device to the cathode interface where it will react. Sputtered nickel oxide (NiO) can also be used as an alternative to PEDOT: PSS with a marked increase in stability (Tran et al., 2022). A similar enhanced lifetime of small molecule solar cells was also obtained with a MoO_3 hole-extraction layer. Substituting PEDOT: PSS with vacuum-deposited MoO_3 as the hole conducting layer enhanced the stability. Since MoO_3 has a greater WF than the majority of the donor materials frequently employed in PSCs, efficient hole extraction at the anode contact is ensured.

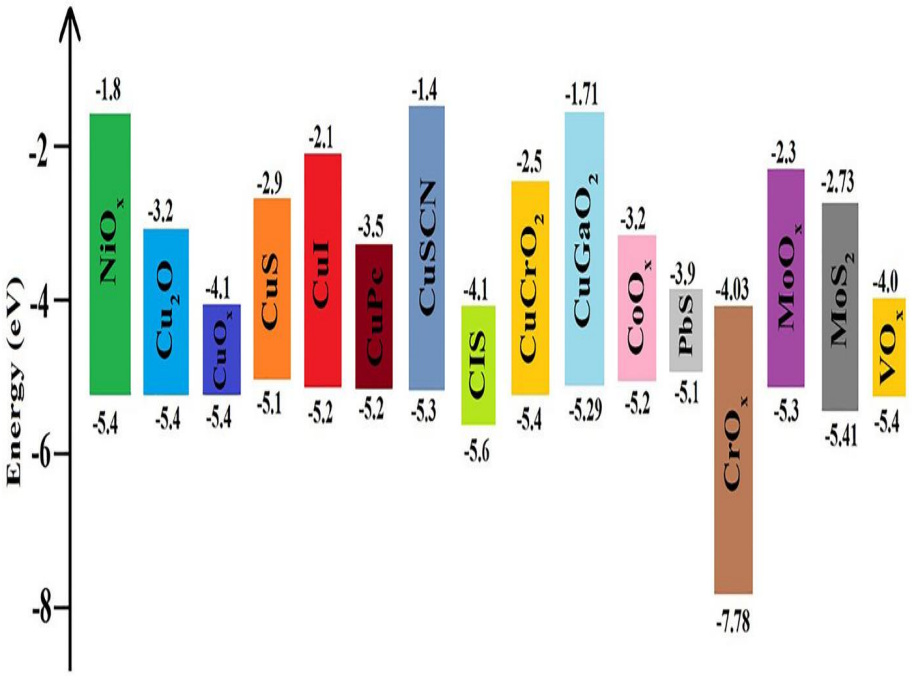

Figure 2.6 Schematics of HTL materials (Nilsson, 2019).

2.4.2 Electron Transport Layer (ETL)

Low WF is a need for a cathode interfacial layer to match the organic acceptor's LUMO and achieve effective charge extraction, electron transport with hole-blocking characteristics, lower energy loss, and fewer interfacial defects. For effective light transmission and sufficient stability to prevent metal electrode migration, the ETL should have transparent inverted devices. High-performance PSCs have used a range of ETL, including low WF metal oxide, composite materials, organic compounds, and polymers.

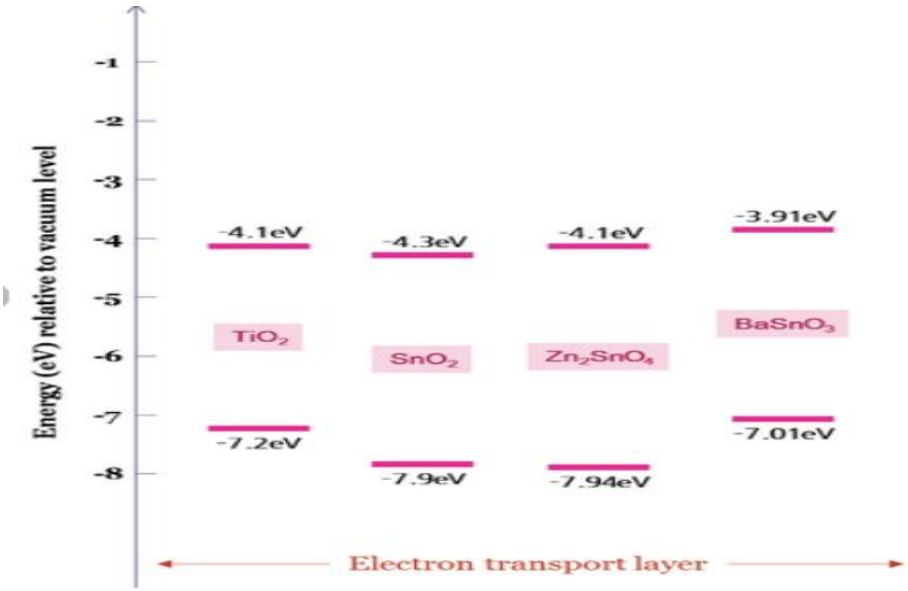

Figure 2.7 Energy band alignment of ETL materials (Mahmood et al., 2017)

i. ZnO as ETL

The photoactive layers absorption will compete with that of the ETL. The photoactive layer can only successfully absorb photons with energies lower than the band gap of the ETL. Fortunately, most of the metal compounds employed in PSCs have high band gaps more than 3eV, resulting in good optical transparency in the visible and near-infrared wavelengths. As ETL materials, n-type metal oxides with low energy levels (4.3 to 4.4 eV) such as TiO_2, ZnO, SnO_2, Al_2O_3, and ZrO_2 were employed (Liu et al., 2016; Yin et al., 2014). The organic molecules HOMO or LUMO level and the metal oxides Fermi level will always coincide. Among those, n-type ZnO is the preferred choice as it offers a desirable band gap and low conduction band minimum (CBM), excellent stability, and high transmittance. These factors make it an ideal candidate for optoelectronic device fabrication (Liu et al., 2019). The low WF of about 4.3 eV is suitable to modify the WF of the ITO in inverted devices. Low optical loss is aided by high transparency throughout the whole visible spectrum, and ZnO band edge cut-off at 375 nm can block UV radiation and shield organic components from photodegradation when exposed to UV light. On the one hand, it is evident that ZnO CBM, at -4.4 eV, is lower than the lowest unoccupied molecular orbital (LUMO), which is found in fullerene derivative acceptors (for instance, -3.9 eV and -3.74 eV for PCBM and ICBA, respectively). This energy level benefits reducing the contact resistance and boosting the parallel resistance by granting ZnO efficient electron extraction and hole blocking capabilities. This means, ZnO ETL can aid

in electron extraction and collection in the fullerene derivative acceptor (Tang et al., 2017; Yip & Jen, 2012). The optical properties of ZnO can be tuned by preparation method, composition, film morphology, and thickness of the layer. ZnO is made using vacuum deposition techniques, which have the advantages of offering a large selection of substrates, good control over film thickness, and smooth film morphology. But because they need expensive and complicated vacuum equipment, vacuum-based processes like thermal evaporation, electron-beam evaporation, or hot filament vapor deposition are not as useful for making low-cost, large-area devices. Consequently, promising ZnO that can be processed in a solution and have the advantages of being inexpensive and highly stable. It is therefore crucial to introduce the solution processing methods.

The most widely used solution preparation method of ZnO for PSCs applications is sol-gel processing (Yu et al., 2013). It clearly demonstrates the benefits of simplicity, low cost, lower crystallization temperature, and size tunability from sol-gel synthesis. The choice of precursor solution and annealing temperature strongly influence the device performance of sol-gel prepared ZnO. However, ZnO is not very stable in solution and a ligand is usually used to stabilize them (Manor et al., 2012; Sun et al., 2011). Uniform sol-gel-derived ZnO films can be obtained at relatively low annealing temperatures (≤ 200 ° C). These films are much more stable than other solution-processed ZnO films, making them a better choice for use in iPSCs.

In the sol-gel technique, uses a mixture of mono ethanolamine as a stabilizer and zinc acetate [Zn $(OAC)_2$] in 2-methoxy ethanol solvent as precursors, then the prepared solution is coated on a glass substrate. Finally, ZnO thin films with good surface quality, outstanding optical transmittance, and electrical characteristics may be produced. Additionally, this is a cheap procedure that doesn't require high prices or vacuum-related equipment (Amakali et al., 2020; Liang et al., 2012; Zhang et al., 2018).

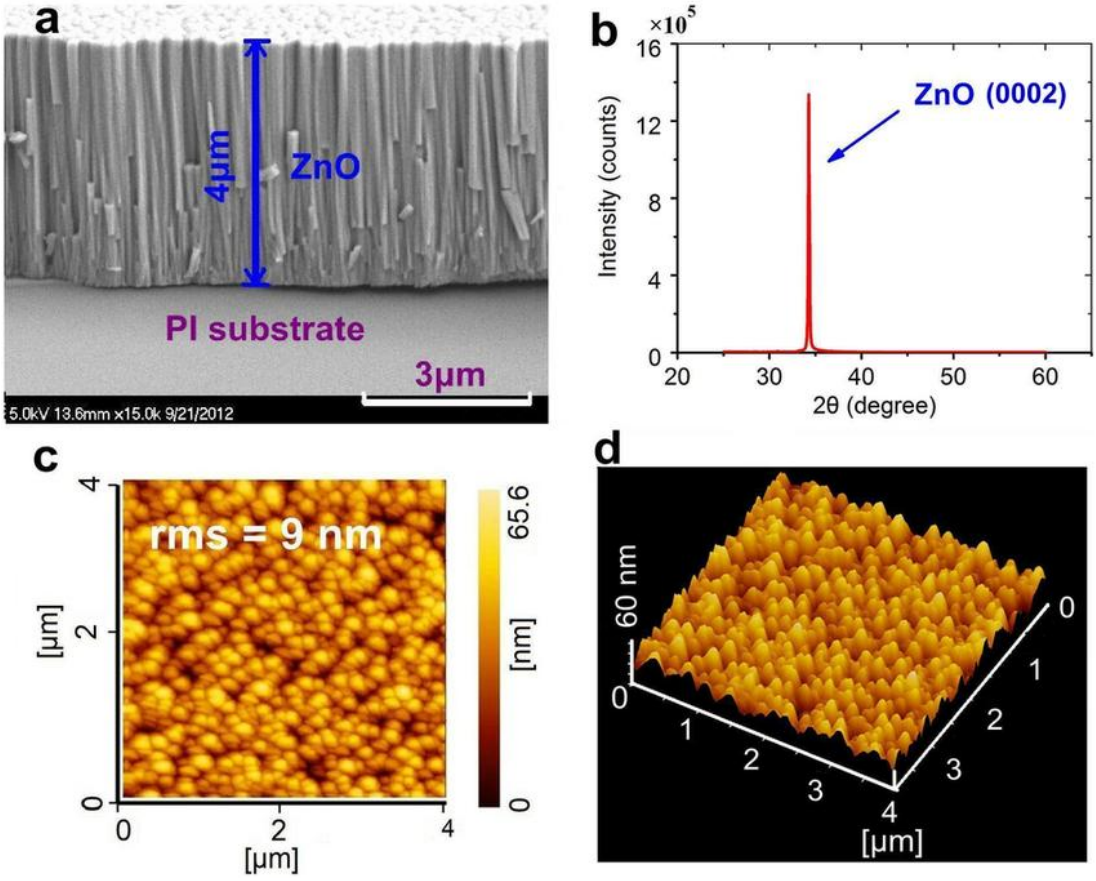

Figure 2.8 images of ZnO thin film a) SEM image of the cross-section, b) XRD pattern of ZnO layer, and c) and d) AFM image (Jin et al., 2013)

The morphology of the ZnO layer is one of the most crucial factors that affect the device's overall performance. There is no "elective" strategy to acquire the ideal morphology, even though various techniques have been devised to deposit a thin ZnO layer on substrates; after all the deposition parameters have been optimized, each technique can produce the optimum results. According to Yu, Xian and their coworkers shows, increasing the surface roughness of the ZnO layer resulted in a 2.08% to 2.88% increase in the power conversion efficiency of a P3HT: PCBM-based iPSCs (Yu et al., 2013). They found both an increase in Jsc and FF for the slowly annealed sample. The boost in the Jsc was explained by the enhanced light absorption, due to the rougher ZnO surface, which should provide an efficient light trapping mechanism: once being scattered by the ZnO layer, the light is reflected by the upper Ag electrode in multiple directions, thus increasing the path length inside the active layer. The higher FF was explained considering the better crystallization of the ZnO, due to the slow annealing rate, which resulted in a more effective electron extraction and hole blocking (Hu et al., 2011). Additionally, it was discovered that series

resistance (R_S) increased with surface roughness and void content in ZnO films. This is because a dense ZnO ETL with a homogeneous surface allowed for the formation of close contact between the ZnO ETL and the BHJ photoactive layer, whereas a rough surface with voids resulted in inferior contact and an increase in cut resistance.

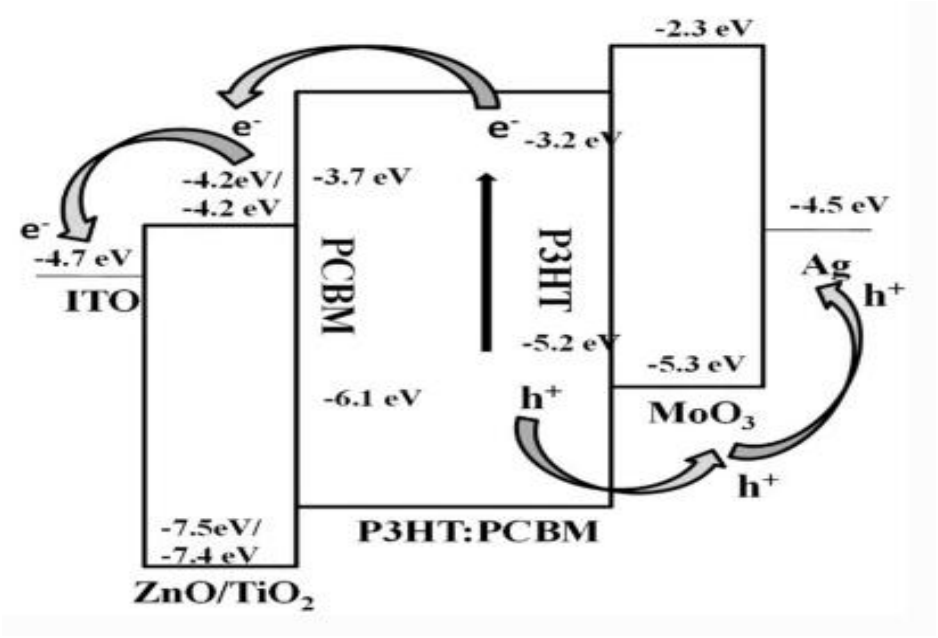

Figure 2.9 Energy level diagram of inverted BHJ PSCs (Shah et al., 2023).

A simple, inexpensive technique for creating various semiconductor thin films is the sol-gel-based spin coating process. This method involves two steps to synthesize thin films: making a sol-gel solution of the precursor and spin coating that solution onto the substrate to produce the desired thin films. For large-area production, which is highly developed in the industry, such a direct liquid deposition technique, which comprises solution, particle, and mixed particle-solution precursors, is very appealing.

Doping of ZnO ETL in inverted polymer solar cells

Most research has gone into finding ways to improve the optical and electrical properties of ZnO semiconductors, as they have great potential for a variety of applications. One approach that has been endorsed is elemental doping, which can efficiently change the properties of the semiconductor. A proper doping of the ZnO layer is another possible route to improve the charge collection efficiency and to reduce the charge recombination, due to charge trapping by defects or oxygen ions. There are several advantages to using doping strategies. They can be used to tailor the electronic structure, reduce defect density,

modify energy levels, and modulate carrier density (Li & Schirra, 2012). Doping semiconductors is an effective method for generating Ohmic contact at the electrode/active layer interface as well as increasing the electrical conductivity of the interfacial layer and tuning the Fermi energy of the semiconductors (Chen et al., 2016). Various elements have been used for doping, such as lithium (Li), aluminum (Al), indium (In), titanium (Ti), and tin (Sn) (Wei et al., 2018; Zhu et al., 2019). Ma and coworkers developed an ETL By doping sol-gel generated ZnO with a 1 wt% perylene derivative PBI-H, in thermally processed ZnO increased the electron mobility by an order of magnitude (5.10×10^{-4} for pure ZnO to 2.02×10^{-3} cm^2 V^{-1} s^{-1}) (Nian et al., 2015). The conductivity also increased to 4.50×10^{-3} S m^{-1}. It is independent of ETL thickness and greater than the device with pure ZnO (7.4 and 8.3%) that PSC devices with PTB7:$PC_{71}BM$ and PTB7- Th: $PC_{71}BM$ photoactive layers created good PCEs of 9.01% and 10.5%, respectively. The WF of modified ITO/ZnO: PBI-H formed good Ohmic contact with $PC_{71}BM$, and lowered to 3.8 eV from 4.2 eV for bare ITO/ZnO, showing enhanced electron population on the conduction band of ZnO. Additionally, it creates nano-fibril networks by non-covalent contacts that are effective for charge transport (Xie et al., 2015).

The device with undoped ZnO had a lower PCE value than the device with sodium quantum dot-doped ZnO (Na-ZnO), but it also showed better light stability. Fang's group and Uddin's group both suggest that doping Al into the ZnO could enhance the device's functionality and stability. For doping of ETLs, the group-III elements such as boron (B) (Tsay & Hsu, 2013), aluminum (Al) (Jun et al., 2012), gallium (Ga) (Zak et al., 2016), and indium (In) (Tang et al., 2017) have been thoroughly researched. The group-III elements could act as an n-type dopant for ZnO to replace Zn sites and produce free electrons. The conductivity of AZO was enhanced by three orders of magnitude compared to neat ZnO.

The group-II elements (alkaline earth), such as magnesium (Mg), strontium (Sr), and barium (Ba), doped ZnO (named as MZO, ZnSrO, and ZnBaO, respectively), have also been added to layers of inverted PSCs in addition to the group III elements (Adam et al., 2020; Pachoumi et al., 2013; Shirdel & Behnajady, 2017). By using amorphous Sr and Ba-doped ZnO ETLs made using the sol-gel processing method, observed better performance and stability of inverted PSCs. In comparison to devices using pure ZnO ETLs, the inverted PSCs based on Sr and Ba-doped ZnO ETL showed greater performance and stability. The reduction in electron trapping on the surface brought about by oxygen

absorption was thought to be the cause of the improvements in device performance brought about by doping ZnO with Sr or Ba. On the ZnO surface, oxygen adsorption at mobile oxygen vacancy sites could be efficiently suppressed or reduced by Sr or Ba doping (Yin et al., 2014).

It was reported a PCE of 8.31% using Mg-doped ZnO as the ETL, which was much higher than that of devices without ETL (3.5%) or with ZnO alone (7.1%) as the ETL. By adjusting the Mg doping level, the WF may be controlled, and the device's stability has also greatly increased. By altering the energy levels without causing any harm to the ZnO nanostructures, the insertion of different metal carbonates, such as Li_2CO_3, K_2CO_3, Na_2CO_3, Cs_2CO_3, and $(NH_4)_2CO_3$, as gradient doping agents for the ZnO layer can enhance the electron extraction capabilities.

It has been discovered that the binary, ternary, and doped states of metal oxides can be employed as effective ETLs in BHJ solar cells as needed. Most notably, flexible substrates and other electronic devices can use low-temperature processing techniques based on the sol-gel approach. According to previous research, doping of zinc oxide ETL such as Mg, Al, Ba, Sr, and many other metals modify the surface of ETL, reduce the defects, and increase the stability and efficiency of BHJ inverted polymer solar cells. The literature cited above demonstrates that metal doping showed better light stability, and improve the pure ZnO's ability for charge transfer while also enhancing the functionality of the device. To date, no research has been conducted to investigate the effect of calcium:ZnO on the performance of P3HT:PCBM BHJ inverted polymer solar cells. So, this study has contributed to understanding the effects of Ca at various concentrations on the solar cell performance of P3HT-based iPSCs.

Table 2.2 Summary of photovoltaic parameters of inverted PSCs

Cathode configuration	Active layer	Anode configuration	Voc/ V	Jsc/mA cm^{-2}	FF (%)	PCE (%)	Ref.
ITO/ZnO	P3HT: PCBM	MoO_3/Ag	0.60	8.73	57.2	3.00	(Huang et al., 2019)
ITO/ZnO	PTB7: PCBM	MoO_3/Ag	0.78	14.28	62.0	6.91	(Huang et al., 2019)
ITO/Al:ZnO	P3HT: PCBM	PEDOT: PSS/Ag	0.61	8.7	68.3	3.63	(Ma et al., 2018)
ITO/Al:ZnO	PTB7: PCBM	MoO_3/Ag	0.74	17.1	70.6	9.07	(Ma et al., 2018)
ITO/Li:ZnO	P3HT: PCBM	MoO_3/Ag	0.61	9.93	68.0	4.07	(Chen et al., 2016)
ITO/Cs:ZnO	P3HT: PCBM	MoO_3/Ag	0.56	10.55	55.0	3.25	(Peng et al., 2015)
ITO/ZnO	P3HT:PCBM	MoO_3/Au	0.60	9.04	60.0	3.17	(Balderrama et al., 2018)
ITO/ZnO	P3HT: PCBM	MoO_3/Ag	0.6	6.94	53.0	2.44	(Kyaw et al., 2008)
ITO/In:ZnO	PCDTBT: PCBM	MoO_3/Al	0.8	12.28	51.7	5.58	(Thambidurai et al., 2014)
ITO/Ga: ZnO	P3HT:PCBM	MoO_3/Au	0.42	11.7	39.7	1.95	(Shin et al., 2010)
ITO/Al: ZnO	P3HT:PCBM	PEDOT:PSS/ Ag	0.54	8.97	55	2.65	(Stubhan et al., 2011)
FTO/In: ZnO	P3HT:PCBM	MoO_3/Ag	0.61	9.935	55	3.3	(Kim et al., 2012)

CHAPTER THREE

3. MATERIALS and METHODS

3.1 Materials and Chemicals

Chemicals

The chemical precursors utilized throughout the experiments include Zinc acetate Dihydrate ($Zn(CH_3CO_2)_2.2H_2O$, Energy Chemical, 99.5%), Calcium chloride hexahydrate ($CaCl_2.6H_2O$, Energy Chemical, 99%), poly(3-hexylthiophene) (P3HT, Sigma-Aldrich), [6,6]-phenyl-C61-butyric acid methyl ester (PCBM, Sigma-Aldrich), 2-methoxy ethanol ($CH_3OCH_2CH_2OH$, Loba Chemicals, 99.5%), monoethanolamine (MEA, CJ Chemicals, 99%), Molybdenum Oxide (MoO_3, Sigma Aldrich), chlorobenzene (Chemical Co, 69%), Acetone (Assay, 99.5%), isopropanol (Dow Chemical, 99.5%), hydrochloric acid (HCl, E & C Chemicals, 37%), Ethanol (Loba Chemicals, 99%), and Distilled water. All chemicals were utilized without any additional purification.

Materials

During the synthesis we used materials like hot plates, beakers, and magnetic stirrers were used for synthesis. Ultrasonic cleaner and UV-ozone cleaner were used to clean ITO coated glass substrate, and the thermal evaporator were used to deposit MoO_3 and Al back electrode.

3.2 Experimental Procedure

3.2.1 Calcium doped ZnO (Ca: ZnO) preparation

To prepare the solutions of pristine ZnO and calcium-doped ZnO ETL, a sol-gel synthesis method was employed. The synthesis process of doping disparate weight ratio (1, 2, 3, 4, and 5) wt% Ca into ZnO precursor solution. Zinc acetate dihydrate ($Zn(CH_3CO_2)_2.2H_2O$) and calcium chloride hexahydrate ($CaCl_2.2H_2O_6$), 2-methoxyethanol, and monoethanolamine (MEA) were used as the starting material, solvent, and stabilizer, respectively. First $Zn(CH_3CO_2)_2.2H_2O$ were dissolved in a mixture of 2-methoxyethanol and monoethanolamine, then after 10 minutes of constant string $CaCl_2.2H_2O_6$ were dissolved in a mixture. The molar ratio of MEA to metal salt was mandated at 1.0 and the

concentration of zinc acetate be 0.5 M. Then, the resulting mixture were stirred for 12 hr. until a clear and transparent homogeneous solution formed. The solution was then aged for 12 hr. at room temperature before being used to increase its viscosity (Huang et al., 2017).

3.2.2 Device fabrication

To prepare the BHJ iPSCs first the patterned ITO glass substrate were washed with soap and thoroughly cleaned using sequential ultrasonic treatments with distilled water, acetone, and isopropanol for 20 minutes each. The cleaned ITO glass substrates were treated with UV-ozone cleaner for 20 minutes before depositing the ZnO films to increase its wettability, then the sol-gel-processed pristine and Ca-doped ZnO films were prepared by spin-coating the precursor solution at 2500 rpm for 30 seconds, and then the as-deposited thin film was annealed at 200°C for 30 minutes. The active layer was prepared from solution of P3HT to PCBM with a ratio (1:1) blend dissolved in chlorobenzene solvent at a concentration of 20 mg/mL after stirring for 6 hours at 80 °C to attain complete dissolution. The prepared solution were spin-coated on top of ZnO and Ca:ZnO ETL at 500 rpm for 10 s, followed by 1000 rpm for 20 s, and then the resulting active-coated substrate were annealed on the hot plate at 130°C for 10 min. Finally, to complete the device, a thin layer of MoO_3 as a hole-transporting layer and Al top electrode were deposited continuously through thermal evaporation under a vacuum. The shadow mask were used during thermal evaporation in a vacuum of 1×10^{-6} Torr, to define the area of 0.04 cm^2. The schematic representation of the overall device fabrication process and device structure ITO/Ca:ZnO/P3HT: $PC_{61}BM/MoO_3$/Al are shown in the Fig. 3.1 below:

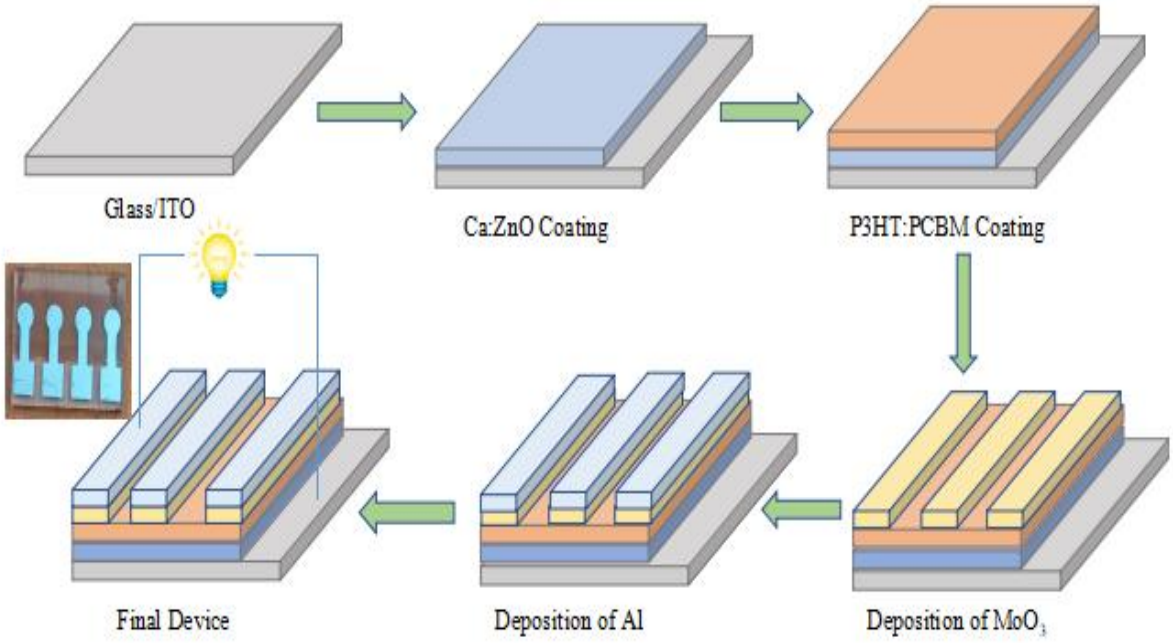

Figure 3.1 Schematic illustration of steps in the fabrication of iPSCs devices

3.2.3 Materials characterization

The morphology and crystal structure of Ca-doped ZnO thin films were determined using scanning electron microscopy (SEM, JCM-6000Plus) and X-ray diffractometer spectroscopy (Shimadzu XRD-7000) at copper K radiation (CuKa = 1.5418Å) respectively. The optical properties of the as-prepared thin films are recorded using a UV-Vis/NIR absorption spectrophotometer and a HORIBA FLUROMAX-4 spectrofluorometric. The electrical conductivity measurements of the pristine ZnO and with Ca dopant films prepared on the ITO substrate were carried out using two probe I-V measurement systems to identify the effect of Ca on the charge conductivity of the electron transport layer (ETL) using probe station equipment. Electrochemical impedance spectroscopy (EIS) were measured to assess charge transfer resistance, and recombination resistance of ETL using a biologic (SP-300) potentiostat. To examine the current-voltage (J-V) characteristics of the iPSC device solar simulator under AM 1.5 illumination with a computer-interfaced Keithley HP2400 source-meter and a solar simulator (model

SS50AAA) to characterize the photovoltaic properties. The Fig. 3.2 illustrate device structure, energy diagram and chemical structure of the photoactive blend.

a)

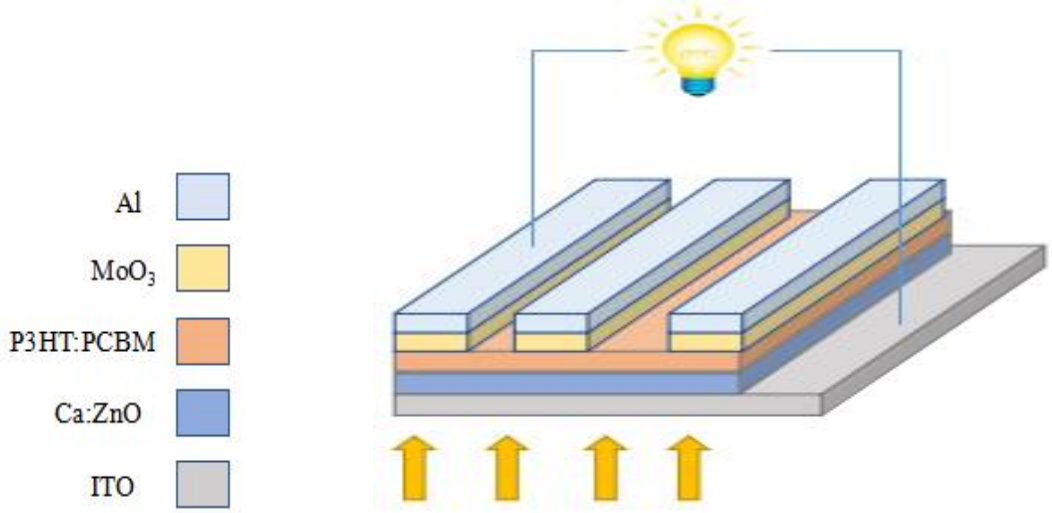

b) c)

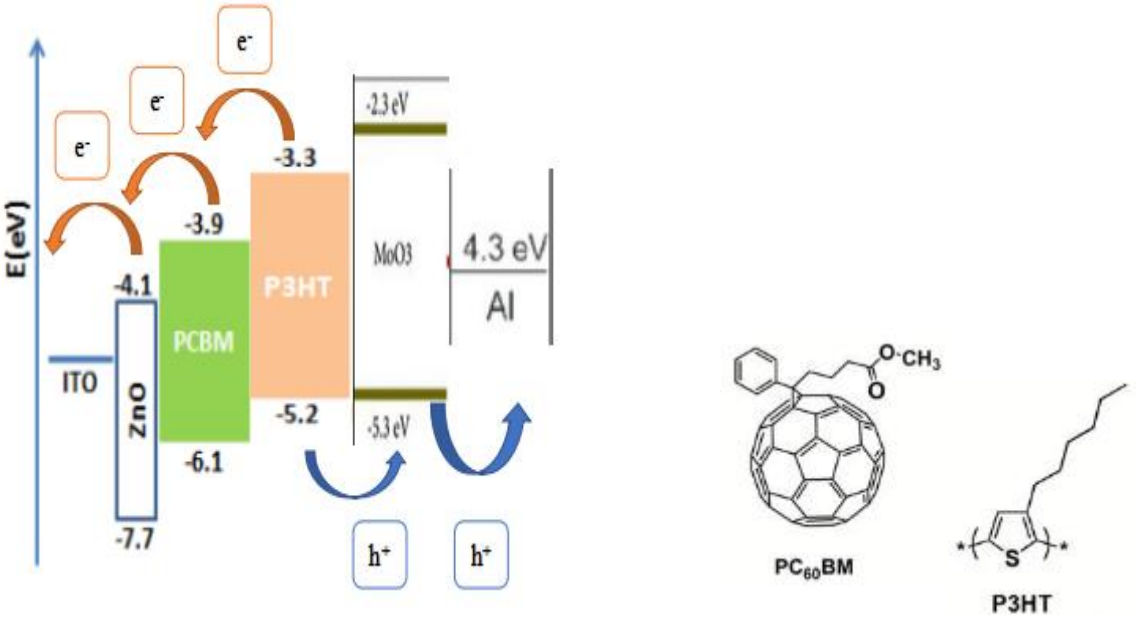

Figure 3.2 a) Schematics of ITO/Ca: ZnO/P3HT: PCBM/MoO3/Al solar cell and b) corresponding energy level diagram, c) chemical structure of PCBM and P3HT

CHAPTER FOUR

4. RESULTS and DISCUSSIONS

4.1 Composition, and Structure of Ca doped ZnO films

4.1.1 XRD Analysis

The crystal structure of ZnO powder and film samples with different Ca concentrations have been investigated by the X-ray diffraction (XRD) method. The peaks of nano powders (NPs) as shown in Fig. 4.1 are indexed at angles of 2θ = 31.74°, 34.38°, 36.22°, 47.74°, 56.54°, 62.8°, 67.88°, and 69°, which corresponds to (100), (002), (101), (102), (110), (103), (200), (112), and (201) planes respectively. All diffraction peaks suggest that the ZnO NPs have a crystalline structure linked to the hexagonal wurtzite phase and it has well concurred with the standard card number (JCPDS File No. 36-1451) (Manikandan et al., 2018). There is no secondary phases like CaO present which could be due to Ca ions were fully dispersed in the host ZnO matrix (introduction of Ca^{2+} ions into ZnO lattice structure and substitution of Zn^{2+}) (Ahmad et al., 2020). However, there is a small peak shift towards lower angles suggesting the incorporation of Ca^{+2} ion into the ZnO lattice, which is commonly ascribed to the increase of the lattice constant (Cao et al., 2013; Slama et al., 2016). This behavior is related to the difference in ionic size between Ca^{2+} (1 Å) and Zn^{2+} (0.74 Å). Because of the increase in residual micro-strain caused by the ion size mismatch, the wurtzite lattice is slightly distorted (Jaballah et al., 2020).

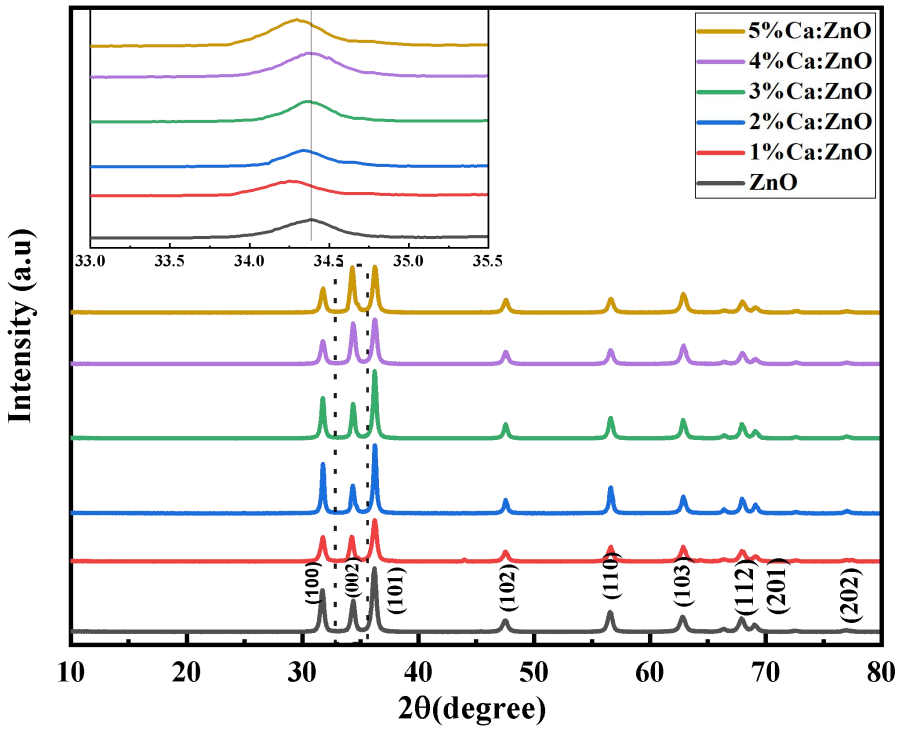

Figure 4.1 XRD patterns of the prepared pristine ZnO and Ca-doped ZnO NPs with different Ca concentrations

The average crystalline size of the sample is calculated from the scherrer equation as shown in below:

$$D = \frac{K\lambda}{\beta\cos\theta} \qquad (3)$$

Where K=0.9 and λ=0.15406

Table 4.1 Average crystalline size of Ca:ZnO

Ca conc. (wt%)	D (nm)
0	21
1	22
2	24
3	25
4	29
5	32

Fig 4.2 shows the XRD peaks of pristine ZnO film and ZnO with different Ca concentrations. During the film annealing process, planes (002) and (110) grain orientation are the preferred directions of crystal formation, which is consistent with past research (Sagar et al., 2007). There is a strong preferential growth orientation along the (002) plane indicating that the films grow perpendicular to the substrate.a lattice plane (002) of ZnO is thermodynamically more favorable because it offers the least surface energy, as a result, the film orientation grows in this (002) plane, resulting in larger grain sizes (Omri et al., 2019). The annealing process also lowers the trap states, enhancing the films crystallinity. In addition, as indicated by the inset plot, all ZnO films on the spectra (002) plane showed a slight shift to the lower diffraction angle after Ca was introduced suggesting the substitution of Zn^{2+} ions with Ca^{2+} inside the lattice was successful. After Ca doping and increasing its concentrations, there is no discernible difference between the peak intensities of all ZnO films and nanoparticle diffraction. This indicates Ca doping in the ZnO structure does not impair its crystallinity, which may be attributed to the lack of stresses resulting from the small size differences between the Zn and the dopant ions and dopant segregation at grain boundaries for high doping concentrations (Jaballah et al., 2020). The broad peak observed in a film at a diffraction angle of around 25° corresponds to the amorphous glass substrate on which the film were deposited.

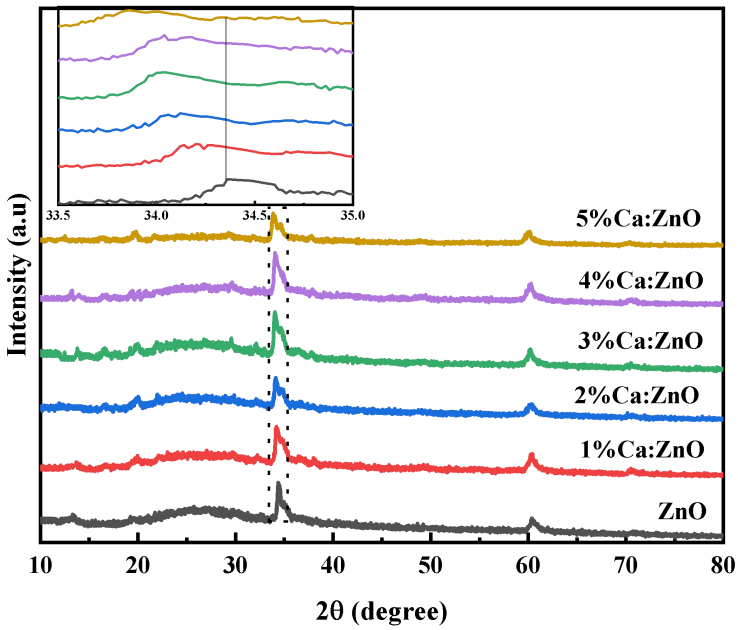

Figure 4.2 XRD pattern of undoped and Ca-doped ZnO with different doping concentrations in films

4.1.2 FTIR Analysis

To determine the chemical compositions of Ca:ZnO films, FTIR spectrum were analyzed from 4000-500 cm^{-1} region. The FTIR spectra of undoped (ZnO) and Ca-doped ZnO thin films (with 3% Ca:ZnO and 5%Ca:ZnO) are shown in Fig. 4.3. The relative functional groups of the various absorption peaks found in the films have been determined. Spectra in the region of 1380 and 1595 cm^{-1} matched the *C=O* bond (Alvarado et al., 2013). A peak of atmospheric CO_2 was identified at 2330 cm^{-1}, whereas the peak at 3436 cm^{-1} were caused by the bending vibration of the *C-H* bond (Ahmad et al., 2020). Ca doping ZnO more frequently improves the abundance of the hydroxyl group due to local ZnO slight lattice distortion. Because of the Ca-O band overlaps with the Zn-O spectral bands in that particular area, the dopant cannot be detected in any doped films. The difference in bond lengths that occurs when the Ca^{2+} ion replaces the Zn^{2+} ion were causing a minor shift to higher wavenumbers (Istrate et al., 2019).

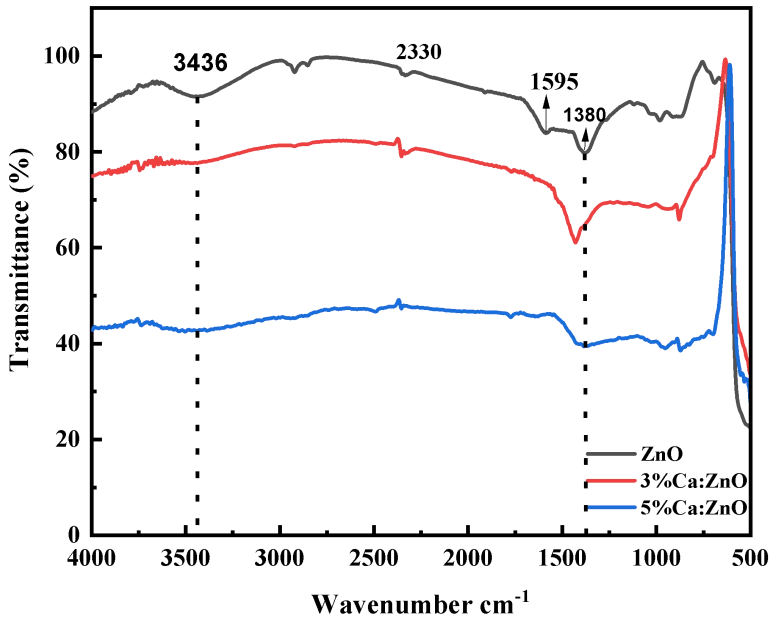

Figure 4.3 FTIR spectra of ZnO,3%Ca: ZnO and 5%Ca: ZnO

4.2 Optical Properties of Ca: ZnO films

4.2.1 UV-Vis Absorption Spectra

The optical absorbance of pristine ZnO and Ca-doped ZnO films with different Ca concentration fluences were measured by ultraviolet-visible (UV-Vis) absorption spectrum within the wavelength range of 300 nm to 800 nm at room temperature as shown in Fig.

4.4 below. The band edge for the pure-ZnO sample appeared at about 367 nm while the band edges of the 1%Ca: ZnO, 2% Ca: ZnO, 3% Ca: ZnO, 4% Ca: ZnO, and 5%Ca: ZnO samples shifted slightly to longer wavelength regions (red shift) after doping as well as the absorption intensity also slightly increase respectively for each sample due to incorporation of calcium into the lattice. The absorbance spectra of the ZnO films as depicted in Fig. 4.4 are appearing to be constant and having small values in the region of the visible and near-infrared spectrum (Vis-NIR) between roughly 400 and 800 nm. The sharp decrement in the absorption edge of ZnO at 370 nm is due to its intrinsic bandgap, which determines the minimum energy required to excite an electron from the valence band to the conduction band, and hence the maximum energy of photons that can be absorbed by the material. Above the bandgap energy, ZnO absorbs light strongly due to inter-band transitions, leading to a sharp decrease in the absorption edge (Tarwal et al., 2014).

All the doped and undoped films show optical absorption spectra only in the ultraviolet (UV) region which is consistent with the transmission spectra. however, the absorption spectra of Ca-doped ZnO show a shift towards lower energies (redshift) compared to undoped ZnO due to the introduction of impurity energy levels into the bandgap of ZnO. The constant improvement in the crystalline quality of the films and the decrease in porosity may be responsible for the absorption edge shifting to a higher wavelength and a rise in sharpness with increasing calcium content (Istrate et al., 2019).

The optical band gap energy (E_g) were determined using the absorbance coefficient calculated from the raw absorbance data. To calculate the band gap values (Eg) of the as prepared samples, Tauc's relationship is applied.

$$\alpha h\nu = A(h\nu - E_g)^{1/2} \qquad (4)$$

Thus, as shown in Fig. 4.4 inset plot, the band gap values have been estimated by extrapolating the linear section of the $(\alpha h\nu)^2$ curve versus the photon energy (eV), where *h* is Plank's constant, *v* is photon frequency, and α is absorption coefficient. Values of the optical band gap for the ZnO films fabricated via the sol–gel method agrees with what is reported previously. The optical bandgap energies for all films with Ca concentrations of (0, 1, 2, 3,4, and 5 %) wt% were 3.31 eV, 3.29 eV, 3.25 eV, 3.21 eV, 3.20 eV, and 3.24 eV, respectively. The band gap decreases with increasing dopant concentration up to

4wt. % Ca doping which could be associated with the merging of an impurity band into the conduction band thereby shrinking the band gap (Girma et al., 2016; Hasabeldaim et al., 2019), then increased when the Ca content were increased to 5 % but still lower than the pristine ZnO film. Formation of such an impurity band gives rise to new donor electronic states just below the conduction band due to hybridization between states of the ZnO matrix and that of the Ca dopants (Girma et al., 2016; Hasabeldaim et al., 2019). The narrowed band gap by Ca, making electron transitions easier at low excitation energies or in longer wavelength regimes. In addition, *Eg* depends on many factors e.g., the granular structure, the nature and concentration of precursors, the structural defects, and the crystal structure of the films (Ahmed et al., 2019). Furthermore, the grain boundary, the stress, and the interaction potentials between defects and host materials in the films influenced the properties of ZnO films.

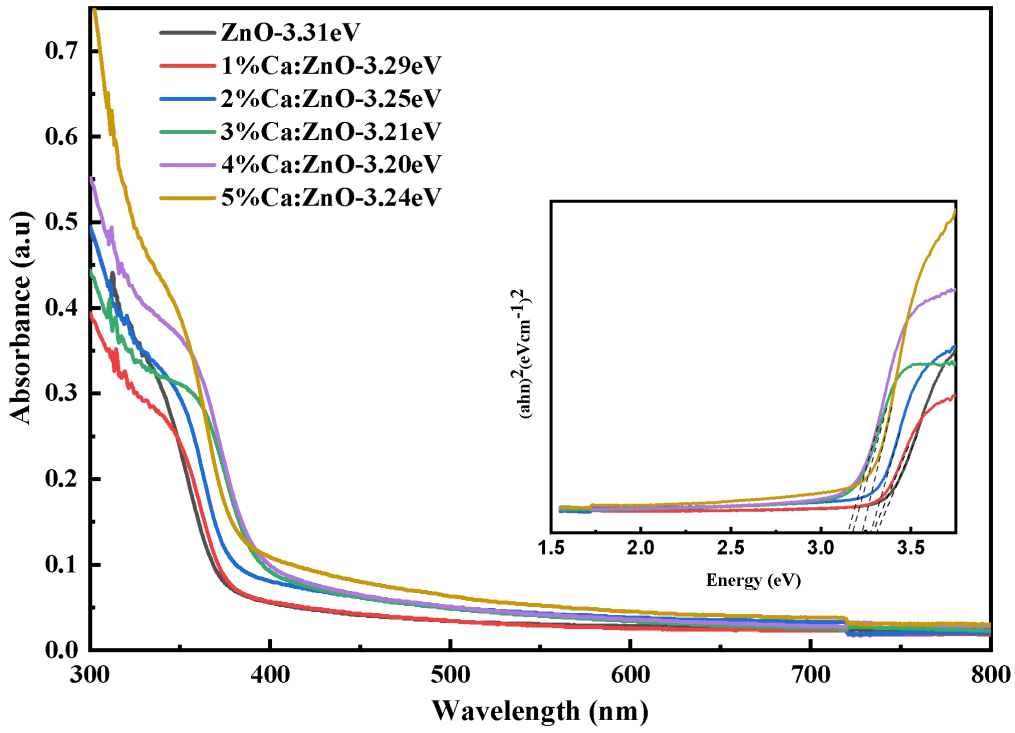

Figure 4.4 Absorbance of ZnO and Ca-doped ZnO film on a glass substrate (with inset Tauc plot)

4.2.2 Optical Transmission Spectra

The optical transmission of the as-prepared Ca: ZnO sample with different Ca concentration coated in a glass substrate were measured to investigate the optical

transmittance of ETLs as shown in Fig. 4.5. All transmittance spectra showed intensive absorption in the UV region, due to the commencement of fundamental absorption. It has seen that all the films are highly transparent over the visible and near-infrared regions from 350 to 800 nm more than 82% with an average transmittance of about 88% for the sol–gel-derived films. With an increase in calcium concentration for 1%Ca: ZnO, 2%Ca: ZnO, 3%Ca: ZnO, 4%Ca: ZnO, and 5%Ca: ZnO, a slight decrease in the average transmission is seen, which is related to an increase in surface roughness (Mahdhi et al., 2015; Sagar et al., 2007). These results show that the calcium-doped ZnO interlayer barely affects the active layer ability to absorb light. Therefore, the visible light can pass through the ITO/ZnO to the polymer active layer without lots of absorption loss. Ca:ZnO can be used as an ETL in inverted polymer solar cells.

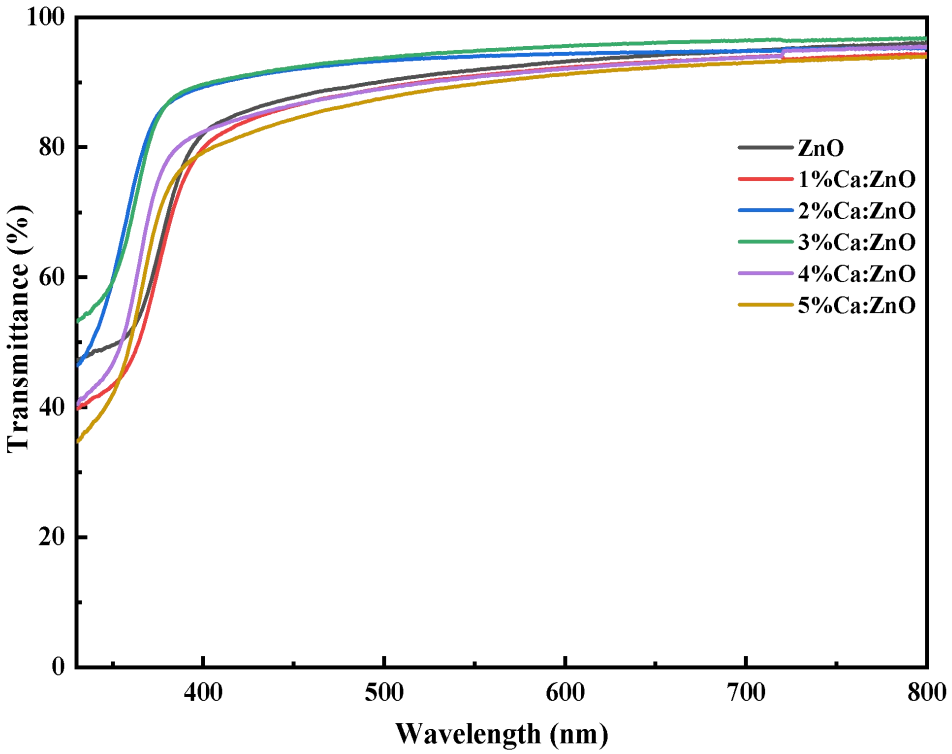

Figure 4.5 Transmittance spectra of as prepared ETL with pure ZnO and Ca doped ZnO films

4.2.3 Photoluminescence (PL) Analysis

By using the photoluminescence method, we were able to determine the interfacial trap passivation of ZnO thin films and analyze the impact of Ca:ZnO ETL (M. Wang et al.,

2019). The PL spectra of samples in a solution and film with various concentration of Ca doping at ambient temperature are measured as shown in Fig 4.6 a) and b) respectively. The PL emission spectra of solutions were measured at the excitation wavelength of 325 nm. It can be observed that all samples demonstrate the emission bands 423 nm (violet emission). The existence of various intrinsic defects, such as O vacancies (V_0), Zn vacancies (V_{Zn}), O interstitials (O_i), Zn interstitials (Zn_i), and O antisites (OZn), is considered to be the cause of the visible emissions multicolored appearance. According to the studies, violet emission results from emissive electron migration from the shallow donor level of Z_{ni} to the top level of VB (Ahmad et al., 2020; Istrate et al., 2021).

In fact, the PL peak intensity has significantly decreased at 3% Ca:ZnO indicates that the ZnO layers defects have been reduced by the addition of Ca, which has improved charge extraction and reduced charge recombination, both of which are helpful for electron transport. The sample with high doping (Ca:ZnO (4% and 5%)), has high PL intensity as result defect centers increase and it may act as a source of electron-hole pair radiative recombination center (El Mir, 2017).

The PL spectra of Ca doped ZnO films as shown in the Fig. 4.6 b) can be seen to emit light in three different bands at wavelengths such as 350nm (band edge emission), 434nm (violet emission), 476nm, and 480nm (blue emission), and 506nm and 524nm (green emission). The intensity of UV emission band at 350nm represents the quenching ability of photogenerated electron-hole pairs. Violet emission at 434nm is attributed to emissive electron migration from the top level of VB to the shallow donor level of Zni (Krishnakumar et al., 2012). The cause of blue emission (476nm and 480nm) is electron migration from a shallow Zni donor level to a neutral V_{Zn} acceptor level (Martha et al., 2014). Blue emission can be attributed to ZnO surface flaws or is presumably caused by V_{Zn}. An increase in peak intensity at (524nm) with Ca doping concentration can act as a source of non-radiative recombination center (Ahmad et al., 2020).

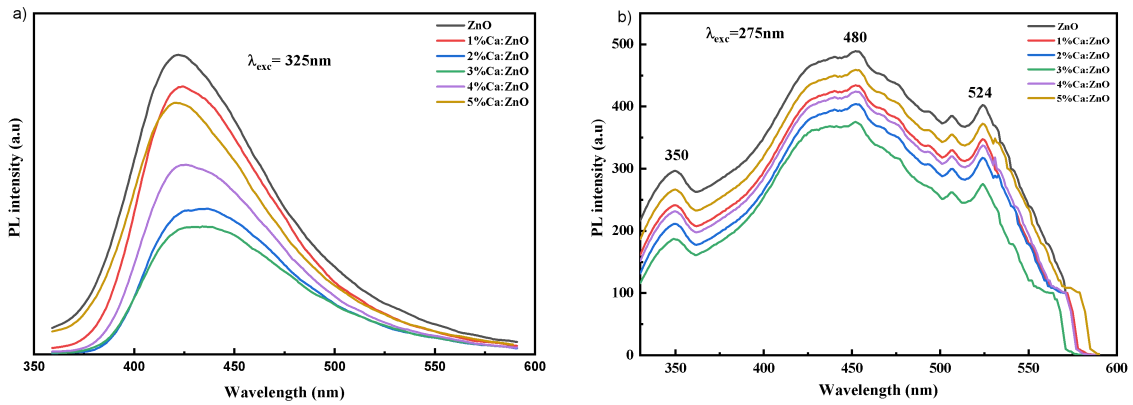

Figure 4.6 Photoluminescence spectra of undoped ZnO and Ca: ZnO in a) solution and b) ITO/Ca:ZnO film on glass substrate

4.3 Electrical and Electrochemical Properties of Ca: ZnO

4.3.1 Electrochemical Impedance Spectroscopy (EIS) Analysis

The interfacial charge transfer dynamics in the ITO/ETL were further investigated using Electrochemical Impedance Spectroscopy. Fig 4.7 shows the EIS Nyquist plots for Ca:ZnO. The EIS experiment data. Nyquist plot was fitted by a Garcia-Belmonte equivalent circuit. The interface layer resistance and charge migration resistance that occur at the interface between ITO/ETL are represented by the arc of the EIS spectra. Low interface layer resistance and high charge migration efficiency are revealed by the smaller arc radius. When Ca is added to ZnO, the semicircle of the Ca: ZnO electrodes is shorter than that of the pristine ZnO electrodes in plots, indicating a reduction in the interfacial resistance (impedance) and charge transfer barrier on the surface (Bembibre et al., 2022). Therefore, doping Ca with ZnO increases the effectiveness of the electron transfer and may help prevent charge recombination (Ahmad et al., 2020). The interfacial resistance decrease dramatically from 114Ω, 91Ω, 58Ω, 38Ω, 33Ω and 24Ω for ZnO, 5%Ca: ZnO, 1%Ca:ZnO, 2%Ca:ZnO, 4%Ca: ZnO and 3% Ca:ZnO respectively. The interface and series resistance is greatly reduced for 3%Ca: ZnO, which has the lowest semicircle arc of all the synthesized thin films, and indicates effective charge carrier separation. EIS confirmed the PL finding of different types of oxygen vacancies and defects, which remarkably supported the charge transfer and separation characteristics of photon-induced charge carriers on the surface of Ca: ZnO films.

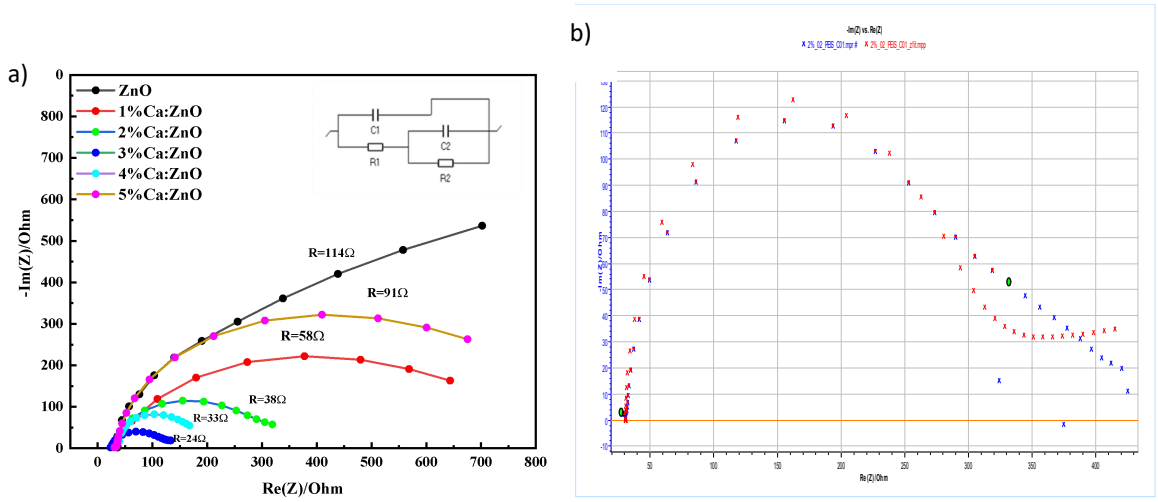

Figure 4.7 the Nyquist plot EIS of pure-ZnO, 1%Ca: ZnO, 2%Ca: ZnO, 3%Ca: ZnO, 4%Ca: ZnO, and 5%Ca: ZnO (inset: equivalent circuit) and b) fitted curve

4.3.2 Electrical conductivity Analysis

Electrical conductivity is another important factor that needs to be considered when designing interfacial layers since materials with high conductivity can minimize the resistance loss of the device. High conductivity can also reduce the voltage drop across the interfacial layers and maximize the internal field across the active film, which can improve field-dependent exciton dissociation.

To investigate the effect of Ca on the electrical conductivity of ZnO, the current-voltage (I-V) characteristics of sandwich devices composed by ITO/ETLs/Al were measured as shown in Fig 4.8 a) and b), and ETL based on ZnO with different Ca concentration. Using the formula below (Eqn. 5), the conductivity of Ca-doped and undoped ZnO devices was estimated from the slope of the I-V plot (Choi et al., 2018).

$$\sigma = G \times \frac{d}{A} \qquad (5)$$

Where σ is the electrical conductivity, G is slope on the I-V curve, d is the thickness of the film (120 nm) and A is the active area (0.04cm^2).

The electrical conductivity of ZnO films is dominated by charges generated from Zn interstitial atoms and oxygen vacancies (Bhat et al., 2010). Therefore, the decrease in resistivity of ZnO films by Ca doping may be due to zinc interstitials and/or oxygen vacancies in the films. Compared with pure ZnO, the films of Ca:ZnO demonstrates a

higher electrical conductivity, it is due to the incorporation of Ca into ZnO improves the electrical conductivity as a result of the substitutional doping of Ca^{2+} at Zn^{2+}sites (Nakrela et al., 2016). In this work, the content 3% Ca:ZnO dopant concentration gave more intense peaks, which underlines the enhancement of the film crystallization. Therefore, this film presents the highest conductivity ($7.5\times10^{-4}Sm^{-1}$). The improved ohmic contact enabled it to be easy to collect electrons and will efficiently hinder the charge recombination of photoinduced electron-hole pairs in ETL. This is responsible for lowering the series resistance of the PSCs device and improving electron transport from the absorber layer to the ITO, both of advantages for photovoltaic performance (Xin et al., 2012).

However, beyond a doping concentration of 3%Ca, there is a segregation of dopant atoms in grain boundary regions that produce disturbances in the charge flow. These defects act as diffusion centers giving rise to different diffusion mechanisms resulting in a sharp decrease in mobility and hence an increase in resistivity. Also, a reduction in mobility or conductivity as increasing the concentration of Ca can be interpreted as calcium oxide-related precipitates, which form at the grain boundaries that may act as scattering centers (Mahdhi et al., 2015).

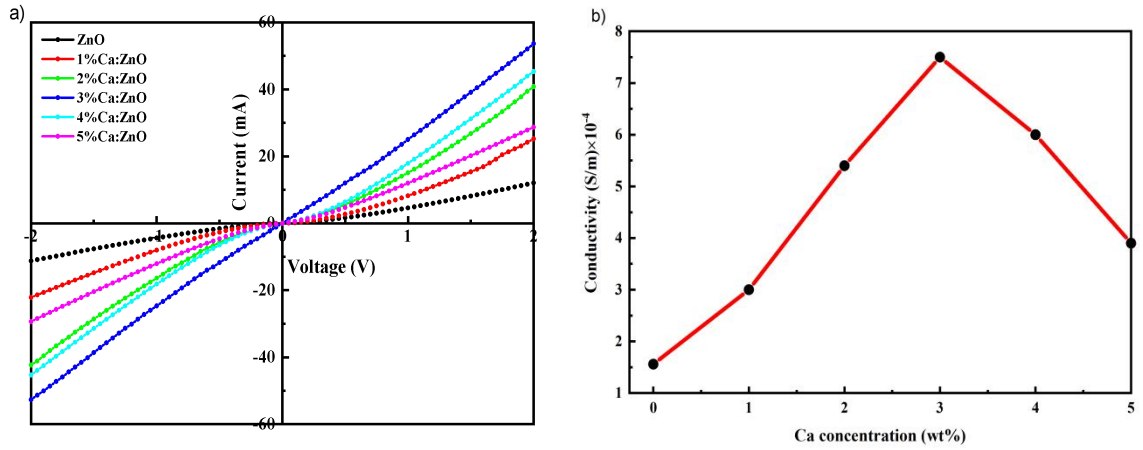

Figure 4.8 a) I-V characteristics of ITO/ETL/Al with ETL (ZnO and Ca: ZnO with different Ca concentration) and b) calculated conductivity Vs Ca concentration

Table 4.2 The conductivity values of different concentration of Ca: ZnO

Ca conc. (wt%)	Conductivity(S/m) $\times 10^{-4}$
0	1.56
1	3.0
2	5.4
3	7.5
4	6.0
5	3.9

4.4 Morphological Properties

To examine the morphology and surface analysis of the scanning electron microscopy (SEM) were used. As shown in Fig. 4.9 ZnO film exhibits the presence of pore on the surface which severely limit device performance via charge carrier recombination. It has been claimed that an increase in surface roughness at 3%Ca doping which improves Jsc because it improves contact between the ZnO ETL and the photoactive layer (Liang et al., 2012). It improves the charge flow resulting an increase conductivity of the ETL and contributed to the enhanced photovoltaic performance of the iPSC. However, further increase the dopant concentration to 5% Ca-doped ZnO causes a drop in charge carrier mobilities and an increase in charge recombination, which lowers *Jsc* because of the higher scattering centers and ZnO surface traps (Chang et al., 2013). It also affects the interface between ETL and active layer. Therefore 5% Ca-doped ZnO loose interface lowers the PCE as compared to 3% Ca-doped ZnO. Fig. 4.9 shows the SEM of both undoped and Ca-doped ZnO thin films.

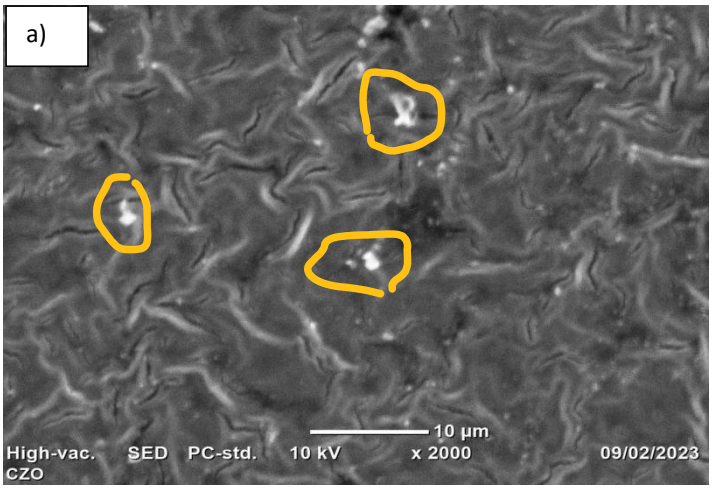

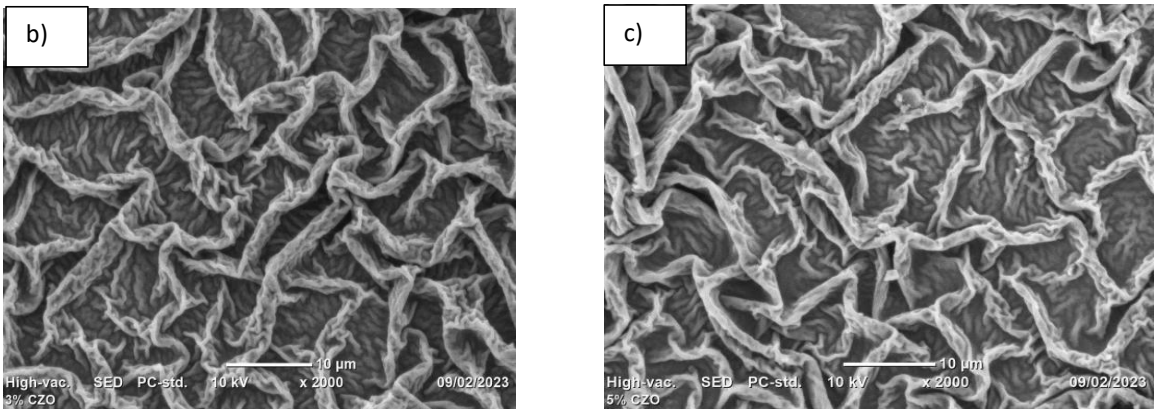

Figure 4.9 SEM image of a) pristine ZnO b)3% Ca:ZnO and c) 5% Ca:ZnO films

4.5 Device performance Measurement

4.5.1 J-V Characteristics

We generally select P3HT:PCBM as the active layer for device fabrication. The optimized photovoltaic performance characteristics introduce the ZnO electron transport layer un-doped and doped with different concentrations of Ca. Fig 4.10a) and b), show the current density-voltage (J-V) curves under AM 1.5 G illumination and in the dark in which iPSCs are constructed using various ETLs (ZnO, 3% Ca:ZnO, and 5% Ca:ZnO). It is evident that doping significantly increased PSCs performance. The reference device with pure ZnO as ETL has shown a maximum PCE of 1.31% with a V_{oc} of 0.38 V, and a J_{sc} of 9.92 mA/cm^2. In general, the quality and thickness of ZnO films play a crucial role in electron transport, which would influence *Jsc* and FF (M. Wang et al., 2019). Meanwhile, the *Voc* were increased from devices with pure ZnO (0.384) to 3% Ca:ZnO (0.647). The enhanced *Voc* is because of the increased built-in field and lowered work function. Due to the relationship between *Voc* and photon energy loss, higher *Voc* indicates less photon energy loss in the Ca:ZnO device, which may be due to a decrease in interface-related recombination or energy loss (Lin et al., 2016). With an increase in the Ca-doping ratio the FF rises from 34.4% for 0% to 38.1% for 5% and 42.29% for 3% doping which is higher than the reference device. Reduced charge recombination and higher shunt resistance (*Rsh*) are the main factors in the enhanced *FF*. It is also enhanced by the optimization of contact between ETL and active layer which is advantageous to the carrier transporting (Lan et al., 2019). When the Ca-doping ratio is 5%, the devices power conversion efficiency is 2.18%, which is significantly higher than the efficiency of the

device with a pristine ZnO ETL (1.31%). In this study, the maximum PCE of 3.25% was achieved by a device containing 3%Ca doping ZnO ETL, which mainly originated from the increase of Jsc. This result is comparable compared to other doped ZnO-based solar cell devices (Liang et al., 2015).

With the increased Ca-doping ratio from 0% to 3%, the Jsc rises from 9.92 mA/cm^2 to 11.88 mA/cm^2 due to the conductivity enhancement of ETL (Huang et al., 2019). *Jsc*, on the other hand, falls with an increasing Ca-doping ratio to 10.6 mA/cm^2 for 5%. Since, with the greater doping ratio of Ca, the excess Ca becomes the scattering center and will reduce the charge carrier mobility (Lin et al., 2016). This is because the *Jsc* value is crucially related to the ZnO thin film mobility. The values of *Jsc*, FF, and PCE were increased by increasing the concentration of calcium from 0 to 3 wt% and then decreased at a high concentration of 5wt% Ca. Additionally, this is in line with the change of series resistance (*Rs*). When the Ca doping ratio is raised to 3%, *Rs* appears to decrease; however, as the doping ratio is raised further, *Rs* increases. Moreover, the device that has 3%Ca: ZnO has a higher *Rsh* which favors an increase in device performance. It is commonly known that the bulk resistance of all interfacial layers throughout the whole PSCs and the contact resistance at interfaces are connected to the Rs value. *Rsh* exposes the loss of charge carriers as a result of current leakage pathways and charge recombination in the bulk or at the interface. A higher shunt resistance corresponds to a lower leakage current since the shunt resistance and leakage current are inversely related. In a polymer solar cell, a high shunt resistance is preferred because it lowers recombination losses and enhances device performance (Cho et al., 2015; Zafar et al., 2017). All devices performance and related parameters are summarized in Table 4.3. The PCE of the device with 3% Ca:ZnO shows more than 147% enhancement comparing with reference device with pristine ZnO ETL.

The dark J-V curves of the devices were recorded to better understand the process underlying the increase in photovoltaic efficiency of devices containing Ca: ZnO. The 3% Ca: ZnO-based device, as shown in Fig. 4.10b), enhances the current flow under forward bias, resulting in superior diode behavior and a higher rectification ratio than pristine ZnO-based iPSCs devices. Compared to pristine ZnO-based devices, the dark leakage current in Ca: ZnO based iPSCs under reverse bias is lower. The lower dark current density suggests that the Ca: ZnO embedded device's current leakage and biomolecular recombination can

be suppressed (Gong et al., 2011). Additionally, the decreased dark current density demonstrates that Ca serves to block the holes at the cathode, increasing the devices efficiency (Schulz et al., 2014). The device's lower leakage current suggests highly effective electron collection.

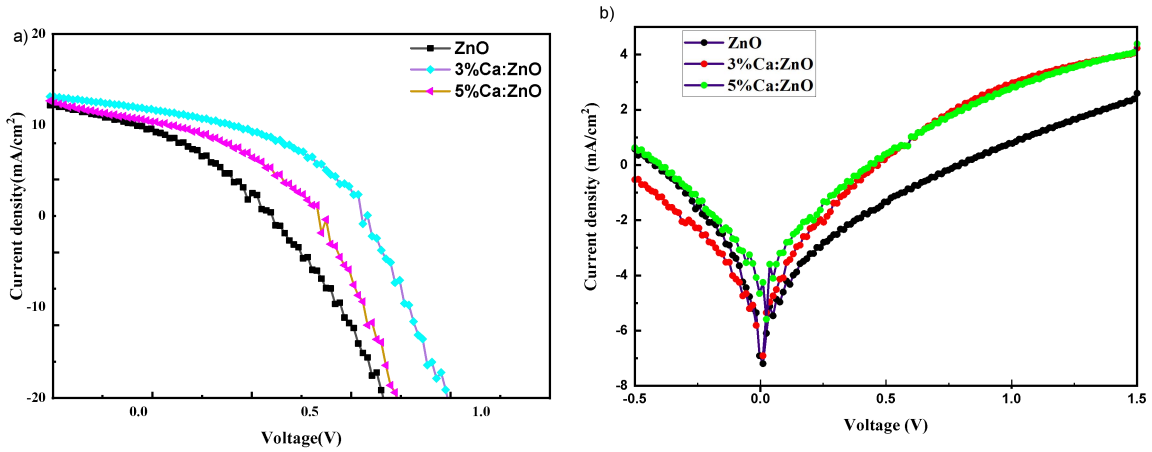

Figure 4.10 a) J–V curves of iPSCs based on P3HT: PCBM with various ETLs. (b) J-V characteristics of corresponding devices in the dark state

Table 4.3 Photovoltaic parameters of iPSCs based on P3HT: $PC_{61}BM$ with various ETL

Ca conc. (wt%)	V_{oc} (V)	J_{sc} (mA/cm^2)	FF (%)	PCE (%)	R_s (Ω.cm^2)	R_{sh} (Ω.cm^2)
0	0.38	9.92	34.44	1.31[a](1.24)[b]	545.40	2342.11
3	0.64	11.88	42.29	3.25[a](3.08)[b]	210.92	4718.83
5	0.53	10.60	38.11	2.18[a](2.04)[b]	601.5	3348

[a] the maximum PCE [b] average PCE of 4 devices

4.5.2 Charge Generation and Exciton Dissociation

Fig. 4.11 depicts the photocurrent density (J_{ph}) as a function of effective voltage (V_{eff}). J_{ph} is calculated by deducting the current density in the dark from the current density under illumination. The voltage where $J_{ph} = 0$ is referred to as the compensation voltage V_o, and

the applied bias V_a is used to determine the voltage that reflects the internal field in the device as (Cowan et al., 2010).

$$V_{eff} = V_o - V_a \quad (6)$$

According to J_{ph}-V_{eff} features, two distinct regions were seen. As shown in Fig 4.11, Jph becomes saturated at a larger voltage (V_{eff} > 0.18V). The excitons are all separated into free charges and collected by the electrodes. It can be shown that the 3%Ca-based PSC has a greater J_{sat} value than the reference device. However, at lower V_{eff}, the device based on Ca:ZnO showed much higher J_{ph}. The charge collection probability (PC) could be estimated by normalizing J_{ph} with J_{ph}, sat (J_{ph}/J_{ph}, sat), and since the Jph, sat values are similar to J_{ph}, Ca: ZnO-based devices were able to achieve higher charge collection efficiency (Huang et al., 2017) and lower field-dependent recombination loss, which accounts for the higher FF and PCE for iPSCs. The more efficient carrier transport directly causes an increase in Jsat and the maximum rate of bound exciton pairs generating per unit volume (Gmax) can be found by:

$$J_{sat} = qG_{max} \times L \quad (7)$$

where L refers to the thickness of the photoactive layer (120nm) and q stands for the elemental charge (Huang et al., 2018). According to the estimates, the values of *Gmax* for devices with ZnO, 3% Ca: ZnO, and 5% Ca: ZnO ETLs are 4.55×10^{24} m^{-3} s^{-1} at *Jsat* of 9.92 mA cm^{-2}, 7.05×10^{24} m^{-3} s^{-1} at *Jsat* of 11.88 mA cm^{-2}, and 5.3×10^{24} m^{-3} s^{-1} at *Jsat* of 10.6 mA cm^{-2} respectively. Adding 3% Ca to the device's ZnO ETL increased *Gmax* significantly. The parameters are summarized in the Table 4.3 below.

Photo-generated excitons must be properly quenched at the donor/acceptor interface in BHJ to obtain high performance in PSCs. Because of the excellent exciton quenching in the BHJ, the PL quenching experiment used pure donor material film rather than BHJ blend film (K.-N. Zhang et al., 2021). The photoexcited PL spectra of samples with the structure ITO/ETL/P3HT excited at 520 nm are shown in Fig 4.11 b). The PL intensity of the P3HT film was much higher due to maximum exciton recombination caused by the lack of an exciton dissociation route. The samples containing 3% Ca:ZnO exhibit substantially lower PL intensity than a pristine ZnO ETL, indicating greater exciton

quenching at the ETL/active layer interface, which may contribute to an improvement in Jsc. Peak intensity was also significantly reduced in P3HT with varied concentrations of ETLs. This PL quenching generated efficient charge transfer at the interface.

The PL quenching efficiency (QE) is calculated as:

$$\text{QE}\ (\%)\ = 1 - \frac{\text{PLblend}}{\text{PLpolymer}}\mathbf{X100} \qquad (8)$$

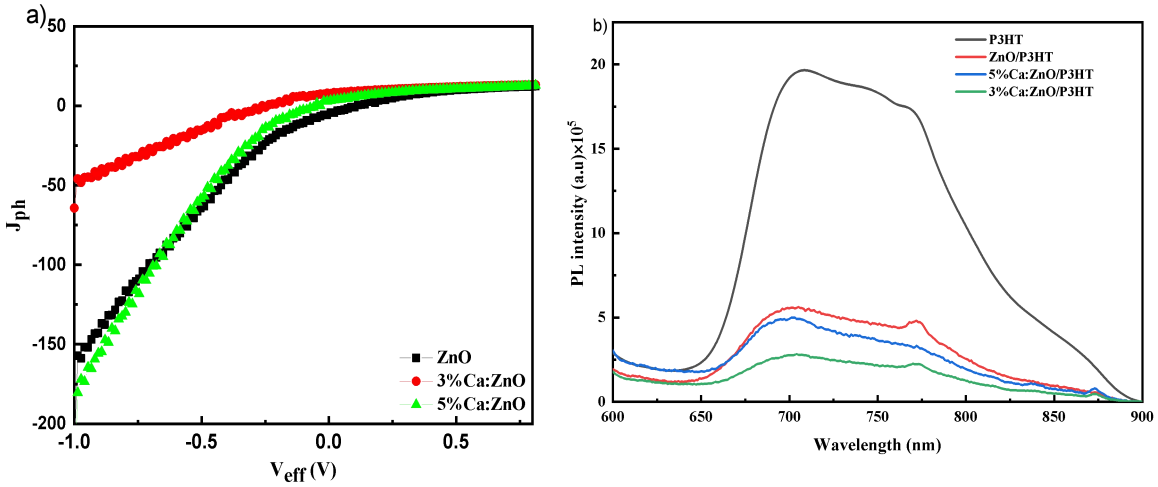

Figure 4.11 a) Jph vs Veff characteristics of PSC b) PL spectra of Glass/P3HT and Glass/ETL/P3HT:PCBM with ETL of pristine ZnO and ZnO with 3% and 5% Ca concentration

Table 4.4 QE, Jsat and Gmax in the fabricated iPSCs

Ca conc. (wt%)	QE (%)	J_{sat} (mA/cm^2)	G_{max} (m^{-3} S^{-1}) ×10^{24}
0	79	9.92	4.55
3	80.5	11.88	7.05
5	78.4	10.6	5.3

4.5.3 Charge Carrier Mobility

The devices short circuit current relies on its free charge mobility as well as exciton creation and quenching. The charge mobility of the device based on a configuration of ITO/Ca: ZnO/P3HT:PCBM/MoO_3/Al with 0%,3% and 5% Ca were determined by fitting the experimental data to the space charge limited current (SCLC) measured under dark

condition using Mott-Gurney model in order to examine the impact of the Ca on the charge transport properties (Yin et al., 2015).

$$\mu=\mu_o \exp(\gamma\sqrt{E}) \quad (9)$$

$$J_{SCLC} = \frac{9}{8}\mu o \mathcal{E}_o \mathcal{E}r \frac{V^2}{L^3} \exp\left(\gamma\sqrt{\frac{V}{L}}\right) \quad (10)$$

In this equation, ε_r stands for relative permittivity of P3HT: PCBM ($\varepsilon r=3$), L for photoactive layer thickness (120nm), γ for field activation factor, J_{SCLC} for space charge limited current density, μo for zero field mobility, V for voltage drop across the film, $\varepsilon_\circ$ for free space dielectric constant ($\varepsilon_\circ = 8.95\times10^{-12}$F/m), and μ for electron mobility. The fittings of SCLC regions of the devices are shown in Fig 4.12, and the charge transport parameters are summarized in Table 4.5.

From the fit curve the extracted charge mobility of the device measured were 2.2×10^{-6}, 9.1×10^{-5}, and 6.7×10^{-5} $cm^2\ V^{-1}\ s^{-1}$ for pristine ZnO, 3%Ca: ZnO and 5%Ca: ZnO P3HT: PCBM based iPSCs device. The maximum electron mobility appears when the device attained 3 wt% Ca concentration. The enhanced charge mobility compensate with the increase in conductivity of ZnO layers after doping. It is demonstrated by reduced Rs and increased FF and Jsc. The negative γ was an indicating that SCLC decreases with increasing the electric field.

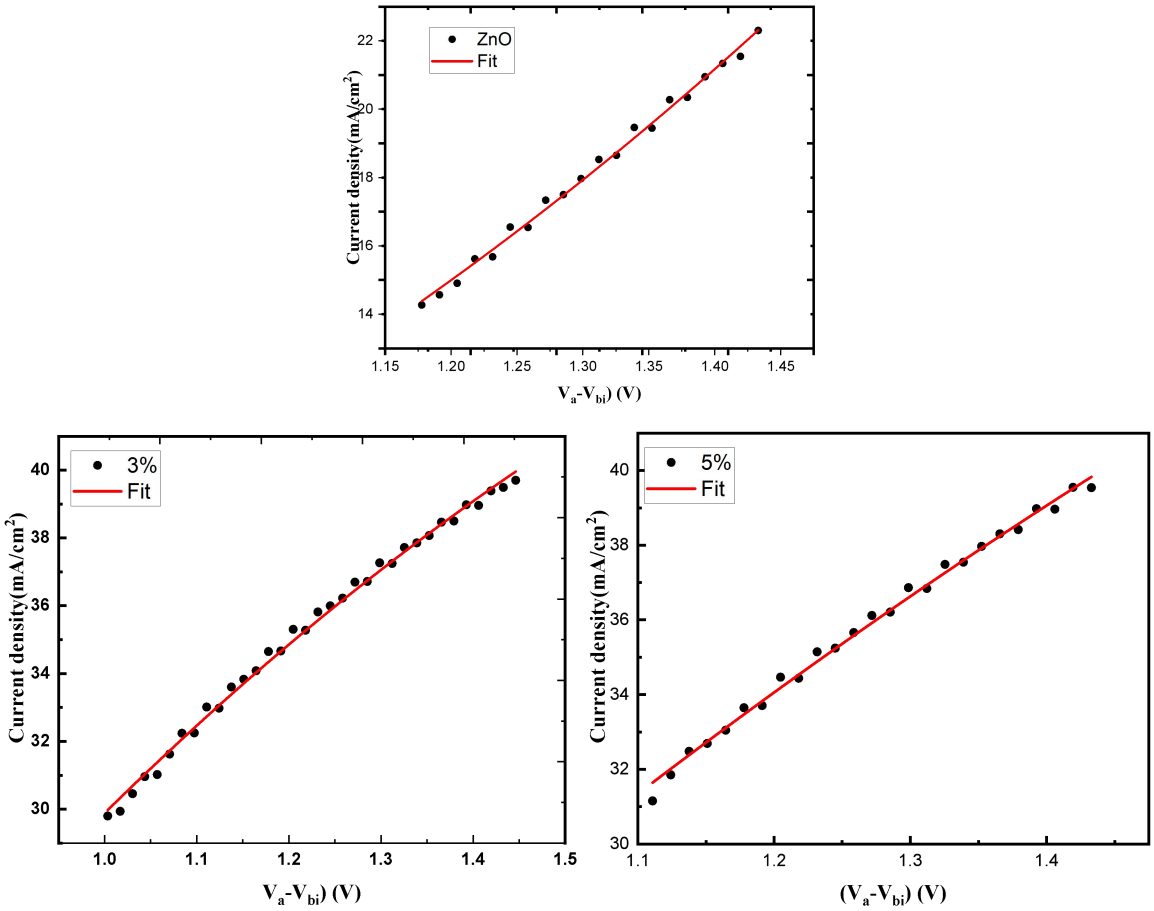

Figure 4.12 The space charge limited current of a device fabricated with ITO/Ca: ZnO/P3HT: PCBM/MoO_3/Al with pristine ZnO and different Ca concentration. The red lines are the fit curve from Mott-Gurney model

Table 4.5 Charge transport parameters of the device with different Ca concentrations

Ca conc. (wt%)	$\mu_o(cm^2V^{-1}s^{-1})$	γ (10^{-4}) $(cm/V)^{1/2}$
0	2.2×10^{-6}	-3.72
3	9.1×10^{-5}	-6.93
5	6.7×10^{-5}	-7.84

5. CONCLUSIONS AND RECOMMENDATIONS

5.1 Conclusions

iPSCs with Pristine and Ca-doped ZnO films were synthesized as electron transport layers using room temperature sol-gel technique. Doping ZnO with Ca modifies the surface morphology, significantly affecting the properties such as conductivity, surface roughness, crystalline structure, and optical characteristics.Ca-doped ZnO usually demonstrate a hexagonal wurtzite structure. It has been observed that the doping results in a rough surface morphology due to the incorporation of calcium into the lattice structure and increase the contact area within the active layer. The size of the particles can be affected. They can become larger or smaller, depending on the level of doping, as compared to the undoped ZnO. Ca-doping of ZnO often improves the material's conductivity, making it appealing for its potential use in transparent conducting films and other electronic devices. It can also change the optical properties of ZnO, altering properties such as photoluminescence, absorption, and bandgap energy. According to the findings, the PCE of iPSCs based on the P3HT: PCBM with 3%Ca: ZnO as ETL exhibits the greatest result (3.25%), which is an improvement of about 147% over pure ZnO (1.31%) as ETL. Solar cell parameters also improved such as the open-circuit voltage (Voc), short-circuit current densities (Jsc) and fill factor (FF). the charge mobility of the device increase with Ca incorporation and reduce exciton recombination ability. These changes can lead to modification in the material's properties, which can be exploited for various applications in electronics, optoelectronics, and other fields.

5.2 Recommendations

Some recommendation based on the findings that helps for future work are:

- More sophisticated technological advancements are required to accurately control the films thickness, morphology and crystallinity.
- Further experiments needed that could examine the effects of other parameters like external quantum efficiency, contact angle and stability.
- Better to use other polymer donor materials with narrow band gap to increase the device performance of iPSCs.
- We also recommend the use of non-fullerene acceptor for the photoactive layer to improve the efficiency of iPSCs.

REFERENCE

Abramavicius, V., Pranculis, V., Melianas, A., Inganäs, O., Gulbinas, V., & Abramavicius, D. (2016). Role of coherence and delocalization in photo-induced electron transfer at organic interfaces. *Scientific reports*, *6*(1), 1-7.

Adam, R. E., Alnoor, H., Pozina, G., Liu, X., Willander, M., & Nur, O. (2020). Synthesis of Mg-doped ZnO NPs via a chemical low-temperature method and investigation of the efficient photocatalytic activity for the degradation of dyes under solar light. *Solid State Sciences*, *99*, 106053.

Ahmad, I., Ahmed, E., Ahmad, M., Akhtar, M. S., Basharat, M. A., Khan, W. Q., Ghauri, M. I., Ali, A., & Manzoor, M. F. (2020). The investigation of hydrogen evolution using Ca doped ZnO catalysts under visible light illumination. *Materials Science in Semiconductor Processing*, *105*, 104748.

Ahmed, M., Meyer, W. E., & Nel, J. M. (2019). Structural, optical and electrical properties of the fabricated Schottky diodes based on ZnO, Ce and Sm doped ZnO films prepared via wet chemical technique. *Materials Research Bulletin*, *115*, 12-18.

Alvarado, J. A., Maldonado, A., Juarez, H., & Pacio, M. (2013). Synthesis of colloidal ZnO nanoparticles and deposit of thin films by spin coating technique. *Journal of Nanomaterials*, *2013*, 167-167.

Amakali, T., Daniel, L. S., Uahengo, V., Dzade, N. Y., & De Leeuw, N. H. (2020). Structural and optical properties of ZnO thin films prepared by molecular precursor and sol–gel methods. *Crystals*, *10*(2), 132.

Andersson, O., & Kemerink, M. (2020). Enhancing Open-Circuit Voltage in Gradient Organic Solar Cells by Rectifying Thermalization Losses. *Solar RRL*, *4*(12), 2000400.

Balderrama, V. S., Sánchez, J. G., Lastra, G., Cambarau, W., Arias, S., Pallarès, J., Palomares, E., Estrada, M., & Marsal, L. F. (2018). High-efficiency organic solar cells based on a halide salt and polyfluorene polymer with a high alignment-level of the cathode selective contact. *Journal of materials chemistry A*, *6*(45), 22534-22544.

Bässler, H., & Köhler, A. (2015). "Hot or cold": how do charge transfer states at the donor–acceptor interface of an organic solar cell dissociate? *Physical Chemistry Chemical Physics*, *17*(43), 28451-28462.

Bembibre, A., Benamara, M., Hjiri, M., Gómez, E., Alamri, H. R., Dhahri, R., & Serra, A. (2022). Visible-light driven sonophotocatalytic removal of tetracycline using Ca-doped ZnO nanoparticles. *Chemical Engineering Journal*, *427*, 132006.

Bhat, J., Patil, A., Swami, N., Mulimani, B., Gayathri, B., Deshpande, N., Kim, G., Seo, M., & Lee, Y. (2010). Electron irradiation effects on electrical and optical properties of sol-gel prepared ZnO films. *Journal of Applied Physics*, *108*(4), 043513.

Borse, K., Sharma, R., Gupta, D., & Yella, A. (2018). Interface engineering through electron transport layer modification for high efficiency organic solar cells. *RSC advances*, *8*(11), 5984-5991.

Cao, L., Jiang, J., & Zhu, L. (2013). Realization of band-gap engineering of ZnO thin films via Ca alloying. *Materials Letters*, *100*, 201-203.

Chambon, S., Derue, L., Lahaye, M., Pavageau, B., Hirsch, L., & Wantz, G. (2012). MoO3 thickness, thermal annealing and solvent annealing effects on inverted and direct polymer photovoltaic solar cells. *Materials*, *5*(12), 2521-2536.

Chang, J., Lin, Z., Zhu, C., Chi, C., Zhang, J., & Wu, J. (2013). Solution-processed LiF-doped ZnO films for high performance low temperature field effect transistors and inverted solar cells. *ACS applied materials & interfaces*, *5*(14), 6687-6693.

Chen, G., Wang, T., Li, C., Yang, L., Xu, T., Zhu, W., Gao, Y., & Wei, B. (2016). Enhanced photovoltaic performance in inverted polymer solar cells using Li ion doped ZnO cathode buffer layer. *Organic Electronics*, *36*, 50-56.

Chen, J. D., Cui, C., Li, Y. Q., Zhou, L., Ou, Q. D., Li, C., Li, Y., & Tang, J. X. (2015). Single-junction polymer solar cells exceeding 10% power conversion efficiency. *Advanced Materials*, *27*(6), 1035-1041.

Cheng, P., Li, G., Zhan, X., & Yang, Y. (2018). Next-generation organic photovoltaics based on non-fullerene acceptors. *Nature Photonics*, *12*(3), 131-142.

Cheng, P., & Yang, Y. (2020). Narrowing the band gap: the key to high-performance organic photovoltaics. *Accounts of chemical research*, *53*(6), 1218-1228.

Cho, H.-S., Shin, N., Kim, K., Kim, B., & Kim, D.-H. (2015). High performance inverted polymer solar cells using ultrathin atomic layer deposited TiO2 films. *Synthetic Metals*, *207*, 31-34.

Choi, J., Jo, J. W., de Arquer, F. P. G., Zhao, Y. B., Sun, B., Kim, J., Choi, M. J., Baek, S. W., Proppe, A. H., & Seifitokaldani, A. (2018). Activated Electron-Transport Layers for Infrared Quantum Dot Optoelectronics. *Advanced Materials*, *30*(29), 1801720.

Choy, W. C. (2012). *Organic solar cells: materials and device physics*. Springer.

Classen, A., Chochos, C. L., Lüer, L., Gregoriou, V. G., Wortmann, J., Osvet, A., Forberich, K., McCulloch, I., Heumüller, T., & Brabec, C. J. (2020). The role of exciton lifetime for charge generation in organic solar cells at negligible energy-level offsets. *Nature Energy*, *5*(9), 711-719.

Cowan, S. R., Roy, A., & Heeger, A. J. (2010). Recombination in polymer-fullerene bulk heterojunction solar cells. *Physical Review B*, *82*(24), 245207.

Devižis, A., Gelzinis, A., Chmeliov, J., Diethelm, M., Endriukaitis, L., Padula, D., & Hany, R. (2021). Carrier tunneling from charge transfer states in organic photovoltaic cells. *Advanced Functional Materials*, *31*(29), 2102000.

Dimitrov, S. D., & Durrant, J. R. (2014). Materials design considerations for charge generation in organic solar cells. *Chemistry of Materials*, *26*(1), 616-630.

El-Ahmar, M., El-Sayed, A.-H. M., & Hemeida, A. (2016). Mathematical modeling of Photovoltaic module and evalute the effect of varoius paramenters on its performance. 2016 Eighteenth International Middle East Power Systems Conference (MEPCON),

El Mir, L. (2017). Luminescence properties of calcium doped zinc oxide nanoparticles. *Journal of Luminescence*, *186*, 98-102.

Elumalai, N. K., Saha, A., Vijila, C., Jose, R., Jie, Z., & Ramakrishna, S. (2013). Enhancing the stability of polymer solar cells by improving the conductivity of the nanostructured MoO 3 hole-transport layer. *Physical Chemistry Chemical Physics*, *15*(18), 6831-6841.

Fanady, B. (2021). *Performance Enhancement of Organic Solar Cells via Device Engineering and Their Future Potential Applications* University of Nottingham].

Feng, B., Zhao, J., Chung, S., Cho, K., Lu, S., Xu, W., & Kan, Z. (2023). Regulating the Donor–Acceptor Interfaces to Reduce Trap Density for Efficient Indoor Organic Solar Cells. *Solar RRL*, *7*(5), 2200989.

Ghiloufi, I., El Ghoul, J., Modwi, A., & El Mir, L. (2016). Preparation and characterization of Ca-doped zinc oxide nanoparticles for heavy metal removal from aqueous solution. *MRS Advances*, *1*(53), 3607-3612.

Girma, T., Siraj, K., & Yifru, A. (2016). Defect induced band gap narrowing of zinc oxide nanoparticles using Li+, Na+ and K+ metal ions as a dopant. *Elixir Mater Sci*, *91*, 38058-38062.

Gnangoin, T. Y., Kassi, D. F., Edjoukou, A. J.-R., Kongrong, O., & Yuqing, D. (2022). Renewable energy, non-renewable energy, economic growth and CO2 emissions in the newly emerging market economies: The moderating role of human capital. *Frontiers in Environmental Science*, 1657.

Gong, X., Tong, M., Brunetti, F. G., Seo, J., Sun, Y., Moses, D., Wudl, F., & Heeger, A. J. (2011). Bulk Heterojunction Solar Cells with Large Open-Circuit Voltage: Electron Transfer with Small Donor-Acceptor Energy Offset (Adv. Mater. 20/2011). *Advanced Materials*, *23*(20), 2271-2271.

Hasabeldaim, E., Ntwaeaborwa, O., Kroon, R., & Swart, H. (2019). Structural, optical and photoluminescence properties of Eu doped ZnO thin films prepared by spin coating. *Journal of Molecular Structure*, *1192*, 105-114.

Hong, L., Yao, H., Cui, Y., Yu, R., Lin, Y. W., Chen, T. W., Xu, Y., Qin, J., Hsu, C. S., & Ge, Z. (2021). Simultaneous improvement of efficiency and stability of organic photovoltaic cells by using a cross-linkable fullerene derivative. *Small*, *17*(24), 2101133.

Hu, Z., Zhang, J., Liu, Y., Hao, Z., Zhang, X., & Zhao, Y. (2011). Influence of ZnO interlayer on the performance of inverted organic photovoltaic device. *Solar Energy Materials and Solar Cells*, *95*(8), 2126-2130.

Huang, S., Duan, L., & Zhang, D. (2020). Synergistic optimization of interfacial energy-level alignment and defect passivation toward efficient annealing-free inverted polymer solar cells. *Journal of materials chemistry A*, *8*(36), 18792-18801.

Huang, S., Tang, Y., Yu, A., Wang, Y., Shen, S., Kang, B., Silva, S. R. P., & Lu, G. (2018). Solution-processed SnO2 nanoparticle interfacial layers for efficient electron transport in ZnO-based polymer solar cells. *Organic Electronics*, *62*, 373-381.

Huang, X., Lv, L., Hu, Y., Lou, Z., Hou, Y., & Teng, F. (2017). Enhanced performance in inverted polymer solar cells employing microwave-annealed sol-gel ZnO as electron transport layers. *Organic Electronics*, *42*, 107-114.

Huang, X., Yu, H., Shi, S., & Huang, C. (2019). Improving the performance of inverted polymer solar cells by the efficiently doping and modification of electron transport layer-ZnO. *Organic Electronics*, *65*, 311-320.

Ibn-Mohammed, T., Koh, S., Reaney, I., Acquaye, A., Schileo, G., Mustapha, K., & Greenough, R. (2017). Perovskite solar cells: An integrated hybrid lifecycle assessment and review in comparison with other photovoltaic technologies. *Renewable and Sustainable Energy Reviews*, *80*, 1321-1344.

Ismail, A., Mamat, M., Banu, I. S., Amiruddin, R., Malek, M., Parimon, N., Zoolfakar, A., Sin, N. M., Suriani, A., & Ahmad, M. (2019). Structural modification of ZnO nanorod array through Fe-doping: ramification on UV and humidity sensing properties. *Nano-Structures & Nano-Objects*, *18*, 100262.

Istrate, A.-I., Mihalache, I., Romanitan, C., Tutunaru, O., Vulpe, S., Nastase, F., & Veca, L. M. (2021). Ca-doped ZnO: Al thin films: Synthesis and characterization. *Coatings*, *11*(9), 1023.

Istrate, A.-I., Nastase, F., Mihalache, I., Comanescu, F., Gavrila, R., Tutunaru, O., Romanitan, C., Tucureanu, V., Nedelcu, M., & Müller, R. (2019). Synthesis and characterization of Ca doped ZnO thin films by sol–gel method. *Journal of Sol-Gel Science and Technology*, *92*, 585-597.

Ito, S., Hirata, T., Mori, D., Benten, H., Lee, L.-T., & Ohkita, H. (2013). Development of polymer blend solar cells composed of conjugated donor and acceptor polymers. *Journal of Photopolymer Science and Technology*, *26*(2), 175-180.

Jaballah, S., Benamara, M., Dahman, H., Lahem, D., Debliquy, M., & El Mir, L. (2020). Formaldehyde sensing characteristics of calcium-doped zinc oxide nanoparticles-based gas sensor. *Journal of Materials Science: Materials in Electronics*, *31*, 8230-8239.

Jarosz, G., Marczyński, R., & Signerski, R. (2022). Efficiency of exciton splitting in organic photovoltaic cells within EQE spectrum. *Applied Surface Science*, *580*, 152167.

Jin, H., Zhou, J., He, X., Wang, W., Guo, H., Dong, S., Wang, D., Xu, Y., Geng, J., & Luo, J. (2013). Flexible surface acoustic wave resonators built on disposable plastic film for electronics and lab-on-a-chip applications. *Scientific reports*, *3*(1), 1-8.

Jørgensen, M., Norrman, K., Gevorgyan, S. A., Tromholt, T., Andreasen, B., & Krebs, F. C. (2012). Stability of polymer solar cells. *Advanced Materials*, *24*(5), 580-612.

Jun, M.-C., Park, S.-U., & Koh, J.-H. (2012). Comparative studies of Al-doped ZnO and Ga-doped ZnO transparent conducting oxide thin films. *Nanoscale research letters*, *7*(1), 1-6.

Khalate, S., Kate, R., & Deokate, R. (2018). A review on energy economics and the recent research and development in energy and the Cu2ZnSnS4 (CZTS) solar cells: A focus towards efficiency. *Solar Energy*, *169*, 616-633.

Khordehgah, N., Guichet, V., Lester, S. P., & Jouhara, H. (2019). Computational study and experimental validation of a solar photovoltaics and thermal technology. *Renewable Energy*, *143*, 1348-1356.

Kim, H. P., bin Mohd Yusoff, A. R., Ryu, M. S., & Jang, J. (2012). Stable photovoltaic cells based on graphene oxide/indium zinc oxide bilayer anode buffer. *Organic Electronics*, *13*(12), 3195-3202.

Krishnakumar, B., Subash, B., & Swaminathan, M. (2012). AgBr–ZnO–An efficient nano-photocatalyst for the mineralization of Acid Black 1 with UV light. *Separation and Purification Technology*, *85*, 35-44.

Kyaw, A., Sun, X., Jiang, C., Lo, G., Zhao, D., & Kwong, D. (2008). An inverted organic solar cell employing a sol-gel derived ZnO electron selective layer and thermal evaporated MoO 3 hole selective layer. *Applied Physics Letters*, *93*(22), 221107.

Lan, W., Liu, Y., Wu, B., Xu, B., Pu, H., Wei, B., Peng, Y., Tian, W., & Zhu, F. (2019). Effect of ZnO electron extraction layer on charge recombination and collection properties in organic solar cells. *ACS Applied Energy Materials*, *2*(10), 7385-7392.

Landrigan, P. J., Fuller, R., Acosta, N. J., Adeyi, O., Arnold, R., Baldé, A. B., Bertollini, R., Bose-O'Reilly, S., Boufford, J. I., & Breysse, P. N. (2018). The Lancet Commission on pollution and health. *The lancet*, *391*(10119), 462-512.

Lattante, S. (2014). Electron and hole transport layers: their use in inverted bulk heterojunction polymer solar cells. *Electronics*, *3*(1), 132-164.

Le Donne, A., Trifiletti, V., & Binetti, S. (2019). New earth-abundant thin film solar cells based on chalcogenides. *Frontiers in chemistry*, *7*, 297.

Lee, K. M., Lai, C. W., Ngai, K. S., & Juan, J. C. (2016). Recent developments of zinc oxide based photocatalyst in water treatment technology: a review. *Water research*, *88*, 428-448.

Li, L., & Schirra, J. S. (2012). H. Cheun, B. Kippelen, OLA Monti, and J.-L. Bredas. *Chemistry of Materials*, *24*, 3044.

Li, Q., Wang, L.-M., Liu, S., Zhan, X., Zhu, T., Cao, Z., Lai, H., Zhao, J., Cai, Y., & Xie, W. (2019). Impact of donor–acceptor interaction and solvent additive on the

vertical composition distribution of bulk heterojunction polymer solar cells. *ACS applied materials & interfaces*, *11*(49), 45979-45990.

Liang, Z., Zhang, Q., Jiang, L., & Cao, G. (2015). ZnO cathode buffer layers for inverted polymer solar cells. *Energy & Environmental Science*, *8*(12), 3442-3476.

Liang, Z., Zhang, Q., Wiranwetchayan, O., Xi, J., Yang, Z., Park, K., Li, C., & Cao, G. (2012). Effects of the morphology of a ZnO buffer layer on the photovoltaic performance of inverted polymer solar cells. *Advanced Functional Materials*, *22*(10), 2194-2201.

Lin, Z., Chang, J., Zhang, C., Zhang, J., Wu, J., & Hao, Y. (2016). Low temperature aqueous solution-processed Li doped ZnO buffer layers for high performance inverted organic solar cells. *Journal of Materials Chemistry C*, *4*(25), 6169-6175.

Liu, H., Li, J., Xia, L., Bai, Y., Hu, S., Liu, J., Liu, L., Hayat, T., Alsaedi, A., & Tan, Z. a. (2018). Perfect complementary in absorption spectra with fullerene, nonfullerene acceptors and medium band gap donor for high-performance ternary polymer solar cells. *ACS applied materials & interfaces*, *10*(35), 29831-29839.

Liu, H., Liu, Z. X., Wang, S., Huang, J., Ju, H., Chen, Q., Yu, J., Chen, H., & Li, C. Z. (2019). Boosting organic–metal oxide heterojunction via conjugated small molecules for efficient and stable nonfullerene polymer solar cells. *Advanced Energy Materials*, *9*(34), 1900887.

Liu, Q., Jiang, Y., Jin, K., Qin, J., Xu, J., Li, W., Xiong, J., Liu, J., Xiao, Z., & Sun, K. (2020). 18% Efficiency organic solar cells. *Science Bulletin*, *65*(4), 272-275.

Liu, X., Li, X., Li, Y., Song, C., Zhu, L., Zhang, W., Wang, H. Q., & Fang, J. (2016). High-performance polymer solar cells with PCE of 10.42% via Al-doped ZnO cathode interlayer. *Advanced Materials*, *28*(34), 7405-7412.

Lizin, S., Van Passel, S., De Schepper, E., Maes, W., Lutsen, L., Manca, J., & Vanderzande, D. (2013). Life cycle analyses of organic photovoltaics: a review. *Energy & Environmental Science*, *6*(11), 3136-3149.

Ma, W., Luo, Y., Nian, L., Wang, J., Wen, X., Liu, L., Hanif, M., Xie, Z., & Ma, Y. (2018). Construction of layered structure of anion–cations to tune the work function of aluminum-doped zinc oxide for inverted polymer solar cells. *ACS applied materials & interfaces*, *10*(12), 10513-10519.

Mahdhi, H., Ayadi, Z. B., Gauffier, J., Djessas, K., & Alaya, S. (2015). Effect of sputtering power on the electrical and optical properties of Ca-doped ZnO thin films sputtered from nanopowders compacted target. *Optical Materials*, *45*, 97-103.

Mahdhi, H., Djessas, K., & Ayadi, Z. B. (2018). Synthesis and characteristics of Ca-doped ZnO thin films by rf magnetron sputtering at low temperature. *Materials Letters*, *214*, 10-14.

Mahmood, K., Sarwar, S., & Mehran, M. T. (2017). Current status of electron transport layers in perovskite solar cells: materials and properties. *RSC advances*, *7*(28), 17044-17062.

Manikandan, B., Endo, T., Kaneko, S., Murali, K., & John, R. (2018). Properties of sol gel synthesized ZnO nanoparticles. *Journal of Materials Science: Materials in Electronics*, *29*, 9474-9485.

Manor, A., Katz, E. A., Tromholt, T., & Krebs, F. C. (2012). Enhancing functionality of ZnO hole blocking layer in organic photovoltaics. *Solar Energy Materials and Solar Cells*, *98*, 491-493.

Martha, S., Reddy, K. H., & Parida, K. (2014). Fabrication of In 2 O 3 modified ZnO for enhancing stability, optical behaviour, electronic properties and photocatalytic activity for hydrogen production under visible light. *Journal of materials chemistry A*, *2*(10), 3621-3631.

Menke, S. M., Ran, N. A., Bazan, G. C., & Friend, R. H. (2018). Understanding energy loss in organic solar cells: toward a new efficiency regime. *Joule*, *2*(1), 25-35.

Moulé, A. J., & Meerholz, K. (2008). Controlling morphology in polymer–fullerene mixtures. *Advanced Materials*, *20*(2), 240-245.

Muhammad, J. Y. u., Waziri, A. B., Shitu, A. M., Ahmad, U. M., Muhammad, M. H., Alhaji, Y., Olaniyi, A. T., & Bala, A. A. (2019). Recent progressive status of materials for solar photovoltaic cell: A comprehensive review. *Sci. J. Energy Eng*, *7*(4), 77-89.

Nakrela, A., Benramdane, N., Bouzidi, A., Kebbab, Z., Medles, M., & Mathieu, C. (2016). Site location of Al-dopant in ZnO lattice by exploiting the structural and optical characterisation of ZnO: Al thin films. *Results in Physics*, *6*, 133-138.

Nian, L., Zhang, W., Zhu, N., Liu, L., Xie, Z., Wu, H., Würthner, F., & Ma, Y. (2015). Photoconductive cathode interlayer for highly efficient inverted polymer solar cells. *Journal of the American Chemical Society*, *137*(22), 6995-6998.

Nilsson, F. (2019). Hole transport layers in organic solar cells: A study of work functions in nanofilms. In.

Noh, Y. W., Jin, I. S., Kim, K. S., Park, S. H., & Jung, J. W. (2020). Reduced energy loss in SnO 2/ZnO bilayer electron transport layer-based perovskite solar cells for achieving high efficiencies in outdoor/indoor environments. *Journal of materials chemistry A*, *8*(33), 17163-17173.

Omri, K., Alyamani, A., & El Mir, L. (2019). Surface morphology, microstructure and electrical properties of Ca-doped ZnO thin films. *Journal of Materials Science: Materials in Electronics*, *30*, 16606-16612.

Opitz, A., Wagner, J., Brütting, W., Hinderhofer, A., & Schreiber, F. (2009). Molecular semiconductor blends: Microstructure, charge carrier transport, and application in photovoltaic cells. *physica status solidi (a)*, *206*(12), 2683-2694.

Organization, W. H. (2016). Ambient air pollution: A global assessment of exposure and burden of disease.

Oseni, S. O., & Mola, G. T. (2019). Effects of metal-decorated nanocomposite on inverted thin film organic solar cell. *Journal of Physics and Chemistry of Solids*, *130*, 120-126.

Pachoumi, O., Li, C., Vaynzof, Y., Banger, K. K., & Sirringhaus, H. (2013). Improved performance and stability of inverted organic solar cells with sol–gel processed, amorphous mixed metal oxide electron extraction layers comprising alkaline earth metals. *Advanced Energy Materials*, *3*(11), 1428-1436.

Padam, G., Rysankova, D., Portale, E., Koo, B. B., Keller, S., & Fleurantin, G. (2018). *Ethiopia–Beyond connections: energy access diagnostic report based on the multi-tier framework*. World Bank.

Pan, H., Zuo, L., Fu, W., Fan, C., Andreasen, B., Jiang, X., Norrman, K., Krebs, F. C., & Chen, H. (2013). MoO3–Au composite interfacial layer for high efficiency and air-stable organic solar cells. *Organic Electronics*, *14*(3), 797-803.

Peng, H., Xu, W., Zhou, F., Zhang, J., & Li, C. (2015). Enhanced efficiency of inverted polymer solar cells using surface modified Cs-doped ZnO as electron transporting layer. *Synthetic Metals*, *205*, 164-168.

Polat, I., Yilmaz, S., Tomakin, M., & Bacaksiz, E. (2017). Role of Mg doping in the structural, optical, and electrical characteristics of ZnO-based DSSCs. *Turkish Journal of Physics*, *41*(2), 160-170.

Potscavage Jr, W. J., Sharma, A., & Kippelen, B. (2009). Critical interfaces in organic solar cells and their influence on the open-circuit voltage. *Accounts of chemical research*, *42*(11), 1758-1767.

Qu, B., & Forrest, S. R. (2018). Continuous roll-to-roll fabrication of organic photovoltaic cells via interconnected high-vacuum and low-pressure organic vapor phase deposition systems. *Applied Physics Letters*, *113*(5), 053302.

Rasmussen, S., & Pomerantz, M. (2007). Handbook of Conducting Polymers. In*:* (pp. 12-11). CRC Press.

Ratcliff, E. L., Meyer, J., Steirer, K. X., Garcia, A., Berry, J. J., Ginley, D. S., Olson, D. C., Kahn, A., & Armstrong, N. R. (2011). Evidence for near-surface NiOOH species in solution-processed NiO x selective interlayer materials: impact on energetics and the performance of polymer bulk heterojunction photovoltaics. *Chemistry of Materials*, *23*(22), 4988-5000.

Romanin, D., Calandra, M., & Chin, A. W. (2022). Excitonic switching across a Z 2 topological phase transition: From Mott-Wannier to Frenkel excitons in organic materials. *Physical Review B*, *106*(15), 155122.

Sagar, P., Shishodia, P., Mehra, R., Okada, H., Wakahara, A., & Yoshida, A. (2007). Photoluminescence and absorption in sol–gel-derived ZnO films. *Journal of Luminescence*, *126*(2), 800-806.

Sampaio, P. G. V., & González, M. O. A. (2017). Photovoltaic solar energy: Conceptual framework. *Renewable and Sustainable Energy Reviews*, *74*, 590-601.

Sampaio, P. G. V., Gonzalez, M. O. A., de Oliveira Ferreira, P., da Cunha Jacome Vidal, P., Pereira, J. P. P., Ferreira, H. R., & Oprime, P. C. (2020). Overview of printing and coating techniques in the production of organic photovoltaic cells. *International Journal of Energy Research*, *44*(13), 9912-9931.

Schulz, P., Cowan, S. R., Guan, Z. L., Garcia, A., Olson, D. C., & Kahn, A. (2014). NiOX/MoO3 Bi-layers as efficient hole extraction contacts in organic solar cells. *Advanced Functional Materials*, *24*(5), 701-706.

Sekicek, G., & Oral, Z. (2021). Ca doped ZnO thin films by sol-gel dip coating method. AIP Conference Proceedings,

Shah, S. K., Ahmad, I., Shah, J., Haq, T. u., & Hayat, K. (2023). Conventional and metal oxide-based inverted polymer solar cells: a comparative experimental study. *Journal of Electronic Materials*, *52*(2), 1400-1409.

Shin, K.-S., Lee, K.-H., Lee, H. H., Choi, D., & Kim, S.-W. (2010). Enhanced power conversion efficiency of inverted organic solar cells with a Ga-doped ZnO nanostructured thin film prepared using aqueous solution. *The Journal of Physical Chemistry C*, *114*(37), 15782-15785.

Shirdel, B., & Behnajady, M. A. (2017). Sol-gel synthesis of Ba-doped ZnO nanoparticles with enhanced photocatalytic activity in degrading Rhodamine B under UV-A irradiation. *Optik*, *147*, 143-150.

Slama, R., El Ghoul, J., Omri, K., Houas, A., El Mir, L., & Launay, F. (2016). Effect of Ca-doping on microstructure and photocatalytic activity of ZnO nanoparticles synthesized by sol gel method. *Journal of Materials Science: Materials in Electronics*, *27*, 7939-7946.

Sreedharan, A., & Das, B. C. (2022). Effect of semiconducting nature of ZnO interfacial layer on inverted organic solar cell performance. *Journal of Physics D: Applied Physics*, *55*(33), 335103.

Stolterfoht, M., Armin, A., Philippa, B., & Neher, D. (2016). The role of space charge effects on the competition between recombination and extraction in solar cells with low-mobility photoactive layers. *The journal of physical chemistry letters*, *7*(22), 4716-4721.

Stubhan, T., Oh, H., Pinna, L., Krantz, J., Litzov, I., & Brabec, C. J. (2011). Inverted organic solar cells using a solution processed aluminum-doped zinc oxide buffer layer. *Organic Electronics*, *12*(9), 1539-1543.

Sun, Y., Seo, J. H., Takacs, C. J., Seifter, J., & Heeger, A. J. (2011). Inverted polymer solar cells integrated with a low-temperature-annealed sol-gel-derived ZnO film as an electron transport layer. *Advanced Materials*, *23*(14), 1679-1683.

Tang, A., Xiao, Z., Ding, L., & Zhou, E. (2021). ~ 1.2 V open-circuit voltage from organic solar cells. *J Semicond*, *42*, 070202.

Tang, J.-F., Chen, L.-C., Tseng, Z.-L., & Chu, S.-Y. (2017). Indium Doped ZnO Thin Films Prepared by Sol–Gel Technique for Efficient Inverted Type of Polymer Solar Cells. *Journal of Nanoelectronics and Optoelectronics*, *12*(8), 849-852.

Tarwal, N., Gurav, K., Kumar, T. P., Jeong, Y., Shim, H., Kim, I., Kim, J., Jang, J., & Patil, P. (2014). Structure, X-ray photoelectron spectroscopy and photoluminescence investigations of the spray deposited cobalt doped ZnO thin films. *Journal of Analytical and Applied Pyrolysis*, *106*, 26-32.

Thambidurai, M., Kim, J. Y., Kang, C.-m., Muthukumarasamy, N., Song, H.-J., Song, J., Ko, Y., Velauthapillai, D., & Lee, C. (2014). Enhanced photovoltaic performance of inverted organic solar cells with In-doped ZnO as an electron extraction layer. *Renewable Energy*, *66*, 433-442.

Tran, H. N., Lee, H., Park, C. B., Krishna, N. V., Wibowo, F. T. A., Jang, S. Y., Kim, J. Y., & Cho, S. (2022). Solution-Processable Nickel Oxide Hole Transport Layer for a Polymer Donor with a Deep HOMO Level. *Advanced Materials Interfaces*, *9*(27), 2201274.

Tsay, C.-Y., & Hsu, W.-T. (2013). Sol–gel derived undoped and boron-doped ZnO semiconductor thin films: preparation and characterization. *Ceramics International*, *39*(7), 7425-7432.

Vithanage, D. A., Devižis, A., Abramavičius, V., Infahsaeng, Y., Abramavičius, D., MacKenzie, R., Keivanidis, P. E., Yartsev, A., Hertel, D., & Nelson, J. (2013). Visualizing charge separation in bulk heterojunction organic solar cells. *Nature communications*, *4*(1), 2334.

Voroshazi, E., Verreet, B., Buri, A., Müller, R., Di Nuzzo, D., & Heremans, P. (2011). Influence of cathode oxidation via the hole extraction layer in polymer: fullerene solar cells. *Organic Electronics*, *12*(5), 736-744.

Wang, F., Tan, Z. a., & Li, Y. (2015). Solution-processable metal oxides/chelates as electrode buffer layers for efficient and stable polymer solar cells. *Energy & Environmental Science*, *8*(4), 1059-1091.

Wang, M., Sun, Y., Guo, J., Li, Z., Liu, C., & Guo, W. (2019). Alkali metal salts doped ZnO interfacial layers facilitate charge transport for organic solar cells. *Organic Electronics*, *74*, 258-264.

Wang, R., Yuan, J., Wang, R., Han, G., Huang, T., Huang, W., Xue, J., Wang, H. C., Zhang, C., & Zhu, C. (2019). Rational tuning of molecular interaction and energy level alignment enables high-performance organic photovoltaics. *Advanced Materials*, *31*(43), 1904215.

Wang, Y., Jafari, M. J., Wang, N., Qian, D., Zhang, F., Ederth, T., Moons, E., Wang, J., Inganäs, O., & Huang, W. (2018). Light-induced degradation of fullerenes in organic solar cells: a case study on TQ1: PC 71 BM. *Journal of materials chemistry A*, *6*(25), 11884-11889.

Wantz, G., Derue, L., Dautel, O., Rivaton, A., Hudhomme, P., & Dagron-Lartigau, C. (2014). Stabilizing polymer-based bulk heterojunction solar cells via crosslinking. *Polymer international*, *63*(8), 1346-1361.

Wei, J., Ji, G., Zhang, C., Yan, L., Luo, Q., Wang, C., Chen, Q., Yang, J., Chen, L., & Ma, C.-Q. (2018). Silane-capped ZnO nanoparticles for use as the electron transport layer in inverted organic solar cells. *ACS nano*, *12*(6), 5518-5529.

Wei, J., Yin, Z., Chen, S.-C., & Zheng, Q. (2017). Low-temperature solution-processed zinc tin oxide film as a cathode interlayer for organic solar cells. *ACS applied materials & interfaces*, *9*(7), 6186-6193.

Wu, J., Luke, J., Lee, H. K. H., Shakya Tuladhar, P., Cha, H., Jang, S.-Y., Tsoi, W. C., Heeney, M., Kang, H., & Lee, K. (2019). Tail state limited photocurrent collection of thick photoactive layers in organic solar cells. *Nature communications*, *10*(1), 5159.

Xie, Z., & Würthner, F. (2017). Hybrid photoconductive cathode interlayer materials composed of perylene bisimide photosensitizers and zinc oxide for high performance polymer solar cells. *Advanced Energy Materials*, *7*(16), 1602573.

Xie, Z., Xiao, B., He, Z., Zhang, W., Wu, X., Wu, H., Würthner, F., Wang, C., Xie, F., & Liu, L. (2015). Self-assembled perylene bisimide J-aggregates as promising cathode modifiers for highly efficient inverted polymer solar cells. *Materials Horizons*, *2*(5), 514-518.

Xin, H., Subramaniyan, S., Kwon, T.-W., Shoaee, S., Durrant, J. R., & Jenekhe, S. A. (2012). Enhanced open circuit voltage and efficiency of donor–acceptor copolymer solar cells by using indene-C60 bisadduct. *Chemistry of Materials*, *24*(11), 1995-2001.

Yang, M. H., Ko, S.-J., An, N. G., Whang, D. R., Lee, S.-H., Ahn, H., Kim, J. Y., Vak, D., Yoon, S. C., & Chang, D. W. (2020). Roll-to-roll compatible quinoxaline-based polymers toward high performance polymer solar cells. *Journal of materials chemistry A*, *8*(47), 25208-25216.

Yin, Z., Zheng, Q., Chen, S.-C., Li, J., Cai, D., Ma, Y., & Wei, J. (2015). Solution-derived poly (ethylene glycol)-TiO x nanocomposite film as a universal cathode buffer layer for enhancing efficiency and stability of polymer solar cells. *Nano Research*, *8*, 456-468.

Yin, Z., Zheng, Q., Chen, S. C., Cai, D., Zhou, L., & Zhang, J. (2014). Bandgap Tunable Zn1-xMgxO Thin Films as Highly Transparent Cathode Buffer Layers for High-Performance Inverted Polymer Solar Cells. *Advanced Energy Materials*, *4*(7), 1301404.

Yip, H.-L., & Jen, A. K.-Y. (2012). Recent advances in solution-processed interfacial materials for efficient and stable polymer solar cells. *Energy & Environmental Science*, *5*(3), 5994-6011.

Yu, X., Yu, X., Hu, Z., Zhang, J., Zhao, G., & Zhao, Y. (2013). Effect of sol–gel derived ZnO annealing rate on light-trapping in inverted polymer solar cells. *Materials Letters*, *108*, 50-53.

Yuan, J., Zhang, Y., Zhou, L., Zhang, G., Yip, H.-L., Lau, T.-K., Lu, X., Zhu, C., Peng, H., & Johnson, P. A. (2019). Single-junction organic solar cell with over 15% efficiency using fused-ring acceptor with electron-deficient core. *Joule*, *3*(4), 1140-1151.

Zafar, M., Yun, J.-Y., & Kim, D.-H. (2017). Performance of inverted polymer solar cells with randomly oriented ZnO nanorods coupled with atomic layer deposited ZnO. *Applied Surface Science*, *398*, 9-14.

Zahid, S., Rasool, A., Ans, M., Akhter, M. S., Iqbal, J., Al-Buriahi, M., Alomairy, S., & Alrowaili, Z. (2022). Environmentally compatible and highly improved hole transport materials (HTMs) based on benzotrithiophene (BTT) skeleton for

perovskite as well as narrow bandgap donors for organic solar cells. *Solar Energy*, *231*, 793-808.

Zak, A. K., Abd Aziz, N. S., Hashim, A. M., & Kordi, F. (2016). XPS and UV–vis studies of Ga-doped zinc oxide nanoparticles synthesized by gelatin based sol-gel approach. *Ceramics International*, *42*(12), 13605-13611.

Zhang, C., Mumyatov, A., Langner, S., Perea, J. D., Kassar, T., Min, J., Ke, L., Chen, H., Gerasimov, K. L., & Anokhin, D. V. (2017). Overcoming the thermal instability of efficient polymer solar cells by employing novel fullerene-based acceptors. *Advanced Energy Materials*, *7*(3), 1601204.

Zhang, G., Zhao, J., Chow, P. C., Jiang, K., Zhang, J., Zhu, Z., Zhang, J., Huang, F., & Yan, H. (2018). Nonfullerene acceptor molecules for bulk heterojunction organic solar cells. *Chemical reviews*, *118*(7), 3447-3507.

Zhang, J., Liu, W., Zhou, G., Yi, Y., Xu, S., Liu, F., Zhu, H., & Zhu, X. (2020). Accurate determination of the minimum HOMO offset for efficient charge generation using organic semiconducting alloys. *Advanced Energy Materials*, *10*(5), 1903298.

Zhang, K.-N., Jiang, Z.-N., Wang, T., Qiao, J.-W., Feng, L., Qin, C.-C., Yin, H., So, S.-K., & Hao, X.-T. (2021). Exploring the mechanisms of exciton diffusion improvement in ternary polymer solar cells: From ultrafast to ultraslow temporal scale. *Nano Energy*, *79*, 105513.

Zhang, M., Zhu, L., Zhou, G., Hao, T., Qiu, C., Zhao, Z., Hu, Q., Larson, B. W., Zhu, H., & Ma, Z. (2021). Single-layered organic photovoltaics with double cascading charge transport pathways: 18% efficiencies. *Nature communications*, *12*(1), 309.

Zhang, Y., Sajjad, M. T., Blaszczyk, O., Parnell, A. J., Ruseckas, A., Serrano, L. A., Cooke, G., & Samuel, I. D. (2019). Large crystalline domains and an enhanced exciton diffusion length enable efficient organic solar cells. *Chemistry of Materials*, *31*(17), 6548-6557.

Zhao, J., Li, Y., Yang, G., Jiang, K., Lin, H., Ade, H., Ma, W., & Yan, H. (2016). Efficient organic solar cells processed from hydrocarbon solvents. *Nature Energy*, *1*(2), 1-7.

Zhou, K., Xian, K., & Ye, L. (2022). Morphology control in high-efficiency all-polymer solar cells. *InfoMat*, *4*(4), e12270.

Zhou, X., Dong, X., Liu, Y., Wang, W., Wei, W., Chen, J., Liu, T., & Zhou, Y. (2022). Effect of wetting surfactants on the work function of PEDOT: PSS for organic solar cells. *ACS Applied Energy Materials*, *5*(3), 3766-3772.

Zhu, X., Hu, L., Wang, W., Jiang, X., Hu, L., & Zhou, Y. (2019). Reversible chemical reactivity of non-fullerene acceptors for organic solar cells under acidic and basic environment. *ACS Applied Energy Materials*, *2*(10), 7602-7608.

Research Fund Acknowledgement

This research thesis was funded by Adama Science and Technology University under the grant number of ASTU/SM-R/748/23,Adama,Ethiopia